TECHNICAL REPORT STANDARD TITLE PAGE

1. Report No.	2. Government Accession No.	3. Recipient's Catalog No.
CFHR 3-5-73-7-1		

4. Title and Subtitle	5. Report Date
STRENGTH AND STIFFNESS OF REINFORCED RECTANGULAR COLUMNS UNDER BIAXIALLY ECCENTRIC THRUST	January 1976
	6. Performing Organization Code
7. Author(s)	8. Performing Organization Report No.
J. A. Desai and R. W. Furlong	Research Report 7-1
9. Performing Organization Name and Address	10. Work Unit No.
Center for Highway Research The University of Texas at Austin Austin, Texas 78712	11. Contract or Grant No. Research Study 3-5-73-7
	13. Type of Report and Period Covered
12. Sponsoring Agency Name and Address	Interim
Texas State Department of Highways and Public Transportation; Transportation Planning Division P. O. Box 5051 Austin, Texas 78763	14. Sponsoring Agency Code

15. Supplementary Notes

Study conducted in cooperation with the U.S. Department of Transportation, Federal Highway Administration.
Research Study Title: "Design Parameters for Columns in Bridge Bents"

16. Abstract

Compression tests on nine reinforced concrete rectangular columns subjected to constant thrust and biaxially eccentric moments were conducted at the off-campus research facility of The University of Texas, The Civil Engineering Structures Laboratory at Balcones Research Center.

The complex nature of biaxially eccentric thrust and biaxially eccentric deformation is discussed briefly. It is the purpose of this study to report the results of tests performed on the 5 in. × 9 in. rectangular columns. Load measurements, lateral displacements, and longitudinal deformations were monitored through the middle 30 in. length of the 72 in. long specimens.

All columns were reinforced identically with a reinforcement ratio equal to 0.011. The flexural strength of cross sections could be predicted adequately by an elliptical function of ratios between biaxial moment components and uniaxial moment capacities. The ACI recommendation that for skew bending, each component of moment should be magnified according to the stiffness about each principal axis of bending appeared to be a reliable technique only for thrust levels above 40 percent of the short column strength.

This report is the first interim report on Project 3-5-73-7 (Federal No. HPR-1(14)), "Design Parameters for Columns in Bridge Bents."

17. Key Words	18. Distribution Statement
rectangular columns, concrete, compression tests, constant thrust, eccentric moments.	No restrictions. This document is available to the public through the National Technical Information Service, Springfield, Virginia 22161.

19. Security Classif. (of this report)	20. Security Classif. (of this page)	21. No. of Pages	22. Price
Unclassified	Unclassified	78	

Form DOT F 1700.7 (8-69)

STRENGTH AND STIFFNESS OF REINFORCED CONCRETE RECTANGULAR COLUMNS UNDER BIAXIALLY ECCENTRIC THRUST

by

J. A. Desai and R. W. Furlong

Research Report 7-1

Project 3-5-73-7
Design Parameters for Columns in Bridge Bents

Conducted for

Texas
State Department of Highways and Public Transportation

In Cooperation with the
U. S. Department of Transportation
Federal Highway Administration

by

CENTER FOR HIGHWAY RESEARCH
THE UNIVERSITY OF TEXAS AT AUSTIN

January 1976

The contents of this report reflect the views of the authors, who are responsible for the facts and the accuracy of the data presented herein. The contents do not necessarily reflect the official views or policies of the Federal Highway Administration. This report does not constitute a standard, specification, or regulation.

S U M M A R Y

The strength of reinforced concrete columns must be analyzed in terms of axial thrust plus bending moment. The magnitude of thrust remains virtually constant through the length of a bridge pier column, but the magnitude of moment varies throughout the length of the column. Estimates of column capacity must be derived from the cross section strength at the position of maximum moment. Analytic techniques have been developed for predicting moment capacity for any level of axial thrust, and design aids in the form of thrust vs. moment capacity graphs are readily available. The design aids for rectangular columns reveal capacity for moments acting in a plane parallel to the sides of the cross section. Estimates of capacity for moments acting in other, skewed planes have been derived from various proposed combinations of major and minor axis moment capacity. Physical tests of square columns have been used to verify some of the proposed combinations.

The position of maximum moment is almost always at the end of a bridge pier column. The magnitude of the maximum moment is influenced significantly by the bending stiffness of the column. The bending stiffness of columns can be estimated most readily for moments applied in a plane parallel to the sides of the column. The effects of bending stiffness for skewed orientations of moments have been analyzed by combining estimates in the plane of the major and the minor axes of rectangular cross sections. Physical test data regarding skew bending stiffness have been reported for square cross sections.

This report contains physical test data for nine rectangular shaped reinforced concrete column specimens subjected to constant axial thrust and skew bending moments that were increased until failure took place. The test program was planned to reveal data points on a thrust-moment interaction surface. Among the nine specimens, three levels of axial thrust were maintained while moments were applied along three nominal skew angles of 22-1/2, 45, and 67-1/2 degrees. All 5 in. wide by 9 in. thick cross sections contained twelve longitudinal bars that

produced a reinforcement ratio of 1.1 percent. Surface strains were monitored throughout the central 30 in. length of the 72 in. specimens.

Tests revealed that an elliptical function accurately describes skewed moment capacity derived from capacities in the plane of each principal axis. The rectangular stress block tended to underestimate flexural capacities for thrust levels near 60 percent of concentric thrust limit strength P_o. Compression strains at the corner of maximum strain were at least 0.33 percent and as high as 0.48 percent before spalling took place. With a reinforcement ratio as low as 1.1 percent the influence of cracked concrete must be included for flexural stiffness estimates at thrust levels as low as 20 percent of P_o. The present American Concrete Institute Building Code Eq. 10-8, employing 40 percent of a gross concrete cross section stiffness, overestimated the effective minor axis stiffness when thrusts were as low as 0.4 P_o. The alternate Eq. 10-7 employing only 20 percent of the gross concrete cross section stiffness plus the steel stiffness yielded reliably safe predictions of secondary effects based on bending stiffness.

I M P L E M E N T A T I O N

The research reported herein indicates that the strength of rectangular shaped, lightly reinforced (reinforcement ratios near 1 percent), concrete columns subjected to biaxially eccentric thrust can be described by an elliptical interaction surface.

$$\left(\frac{m_x}{M_x}\right)^2 + \left(\frac{m_y}{M_y}\right)^2 = 1 \qquad \text{(A)}$$

in which

m_x = ultimate moment about the x axis

m_y = ultimate moment about the y axis

M_x = moment capacity if the ultimate thrust acted only about the x axis

M_y = moment capacity if the ultimate thrust acted only about the y axis

The design ultimate moments, m_x and m_y, for Eq. (A) should include any secondary effects of column slenderness. The slenderness effect can be estimated adequately by means of the moment magnification relationship, applied independently for each moment about its own axis of bending.

$$\delta = \frac{0.6 + 0.4\,\frac{M_1}{M_2}}{1 - \frac{P_u(k\ell)^2(1+\beta_d)}{\pi^2(0.2E_cI_G + E_sI_s)}} \qquad \text{(B)}$$

for which

δ = moment magnification factor

M_1 = smaller of the nominal design end moments on the column

M_2 = larger of the nominal design end moments on the column

P_u = ultimate design thrust

β_d = ratio between design dead load moment and design total load moment

$k\ell$ = effective length of the column

π = circular constant = 3.1416

E_c = modulus of elasticity for concrete

I_G = moment of inertia of the area bounded by the gross area of concrete

E_s = modulus of elasticity of steel

I_s = moment of inertia of the area of longitudinal reinforcement.

If the uniaxial moment-thrust capacity interaction diagram is normalized by dividing thrusts by the concentric thrust capacity, P_o, and by dividing moments by the maximum moment capacity, M_{max}, the normalized curves for each axis of bending of rectangular cross sections with equal amounts of steel in each of its four faces have virtually the same shape. This phenomenon suggests that initial design should be based upon a resultant moment, M_R, acting about the strong axis of the rectangle, say the x axis, then

$$M_R = \sqrt{m_{u\,x}^2 + (\lambda\, m_{uy})^2} \qquad (C)$$

for which

m_{ux} = design ultimate moment about the strong axis

m_{uy} = design ultimate moment about the weak axis

λ = ratio between the long and the short side of the rectangle.

A B S T R A C T

Compression tests on nine reinforced concrete rectangular columns subjected to constant thrust and biaxially eccentric moments were conducted at the off-campus research facility of The University of Texas, The Civil Engineering Structures Research Laboratory at Balcones Research Center.

The complex nature of biaxially eccentric thrust and biaxially eccentric deformation is discussed briefly. It is the purpose of this study to report the results of tests performed on the 5 in. X 9 in. rectangular columns. Load measurements, lateral displacements, and longitudinal deformations were monitored through the middle 30 in. length of the 72 in. long specimens.

All columns were reinforced identically with a reinforcement ratio equal to 0.011. The flexural strength of cross sections could be predicted adequately by an elliptical function of ratios between biaxial moment components and uniaxial moment capacities. The ACI recommendation that for skew bending, each component of moment should be magnified according to the stiffness about each principal axis of bending appeared to be a reliable technique only for thrust levels above 40 percent of the short column strength.

This report is the first interim report on Project 3-5-73-7 (Federal No. HPR-1(14)), "Design Parameters for Columns in Bridge Bents."

KEY WORDS: rectangular columns, concrete, compression tests, constant thrust, eccentric moments.

TABLE OF CONTENTS

Chapter		Page
I.	INTRODUCTION	1
	1.1 General	1
	1.2 Previous Work on Strength	3
	1.3 Slenderness Effects Under Skew Bending	9
	1.4 Extension of Existing Knowledge	10
II.	TEST MEASUREMENTS	11
	2.1 Specimens	11
	2.2 Materials	13
	2.3 Loading System and Measurement	15
	2.4 Deformation Measurement	20
III.	TEST RESULTS	29
	3.1 General	29
	3.2 Maximum Moments	30
	3.3 Analytic Estimates of Capacity	39
	3.4 Maximum Compression Strain Before Failure	44
	3.5 Stiffness	46
	3.6 Moment Magnification Factors	57
IV.	CONCLUSIONS	63
REFERENCES		65

L I S T O F T A B L E S

Table		Page
2.1	Testing Sequence	13
2.2	Concrete Mix	14
2.3	Compressive Strength	14
2.4	Reinforcement Tests Results	15
2.5	Comparison of Dial Gage and VIDAR Readings, Test Specimen RC-5	27
3.1	Location of Failure	29
3.2	Initial Eccentricities	35
3.3	Summary of Test Results	38
3.4	Moment Magnifier (δ) Using ACI Eq. (10-5)	58
3.5	Comparison of $\delta_{measured}$ Vs. δ_{ACI}	60
3.6	M_R Vs. M_{RACI}	61

L I S T O F F I G U R E S

Figure		Page
1.1	Part Circle Support: Interstate 35, Austin, Texas	2
1.2	Failure Surface S_1	4
1.3	Failure Surface S_2	5
2.1	Test Specimen	12
2.2	Stress-Strain Curve for 6mm ϕ Bar	16
2.3	Schematic Arrangement of Loading Technique	18
2.4	Diagram of Loading Frame	19
2.5	Steel Frame for Positioning Linear Potentiometer	21
2.6	Steel Frame and Potentiometers in Position	22
2.7	Deflection Curves - Thrust Level $0.2P_o$	23
2.8	Deflection Curves - Thrust Level $0.4P_o$	24
2.9	Deflection Curves - Thrust Level $0.6P_o$	25
2.10	Complete Set of Test With all Instruments in Place	28
3.1	RC-2 Weak Axis Deflection	31
3.2	Deflection Readings Correction	33
3.3	Representation of Deflected Shape as Sine Wave	36
3.4	Change in End Eccentricity	37
3.5	Interaction Diagram for Maximum and Minimum Concrete Strength	40
3.6	Strong Axis P/P_o Vs. M/m_{max}	41
3.7	Weak Axis P/P_o Vs. M/m_{max}	42
3.8	Test Results and Analytic Capacity of Rectangular Columns	43
3.9	Prefailure Compressive Strain at Midheight Vs. Maximum Resultant Moment	45

Figure Page

3.10 Curvature Representation 46

3.11 Moment Vs. Average Curvature RC-1 48

3.12 Moment Vs. Average Curvature RC-2 49

3.13 Moment Vs. Average Curvature RC-4 50

3.14 Moment Vs. Average Curvature RC-5 51

3.15 Moment Vs. Average Curvature RC-3 52

3.16 Moment Vs. Average Curvature RC-9 53

3.17 Moment Vs. Average Curvature RC-6 54

3.18 Moment Vs. Average Curvature RC-7 55

3.19 Moment Vs. Average Curvature RC-8 56

CHAPTER I

INTRODUCTION

1.1 General

The structural problem of analysis and design involving axial compression load and biaxial bending occurs in almost every reinforced concrete frame. In building construction the use of biaxially loaded columns cannot be avoided, and in many cases the biaxial load conditions control the requirements for design. Any column designed by the ACI 318-71 Code [1]* must be designed to resist moments about either axis, and ACI 318-71 requires a minimum eccentricity of 1 in. or 0.1 times the thickness of column about either axis for tied columns, but the Commentary [23] specifically states that the minimum eccentricities need not be considered simultaneously. Biaxial eccentricities larger than the minimum are commonly experienced in corner columns of framed structures.

Columns in skewed bridge bents, Fig. 1.1, are subjected to lateral forces in addition to vertical compressive forces. Bridge supports are subjected to braking and acceleration forces in the direction of traffic plus wind forces perpendicular to the traffic in addition to the vertical forces caused by the weight of the structure and traffic. Horizontal deck forces on the columns in bents skewed with respect to traffic flow create combinations of significant eccentric thrust that can act about both principal axes of the columns.

Interest in the ultimate load design of biaxially loaded columns has been directed primarily toward the provision of adequate cross section strength, and most cross sections studied have been square and rectangular in shape.

---

*The number in brackets refers to the list of references at the end of this thesis.

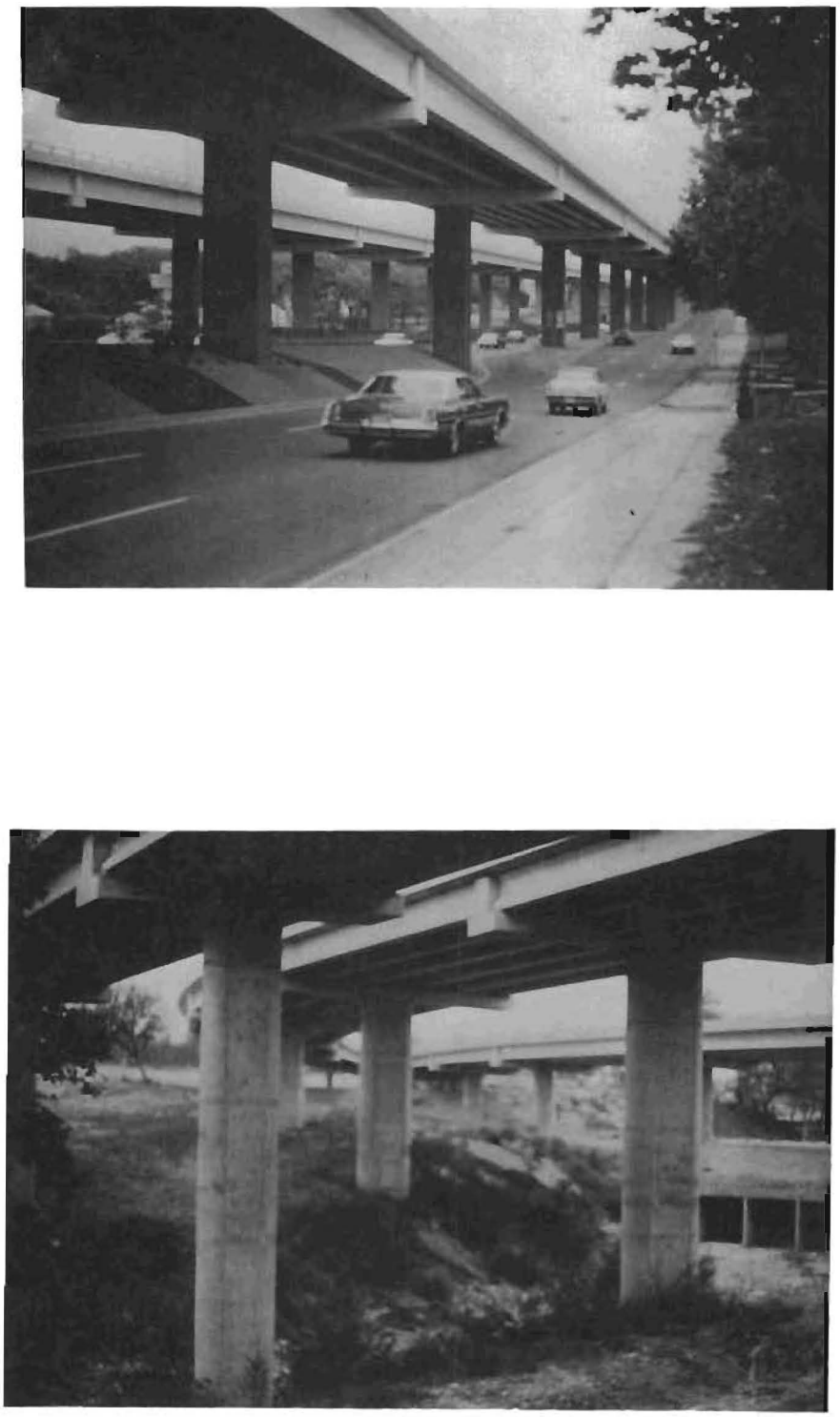

Fig. 1.1. Part circle support: Interstate 35, Austin, Texas.

1.2 Previous Work on Strength

In 1952 Craemer [2] made an attempt to solve the biaxial bending problem using the theory of plasticity, and he proposed a method of analysis. His method was based on adaptations of beam analysis procedures used for ideally plastic behavior.

In 1958 Tung Au [3] generalized the strength equations in a nondimensional form that was consistent with the report of the Joint ACI-ASCE Committee on Ultimate Strength Design [4]. He also developed charts to simplify applications of his equations used for a proposed design procedure. The selection of a specific chart was determined by the way in which the neutral axis intersected the cross section.

Chu and Pabarcius [5] in 1958 developed a method to determine the actual stress and strain distribution for reinforced concrete sections subjected to biaxial bending and compressive load. They applied their procedure by selecting a cross section to resist a specific thrust and assuming a location of the neutral axis. Then compatible stresses in concrete and steel could be determined. A trial and error procedure was followed until the thrust and biaxial moment coincided with acceptable design requirements. The procedure was sensitive to the conditions for which stresses changed from elastic to inelastic behavior.

In 1960 Bresler [6] proposed two equations for the solution of the skew bending problem. His equations were for short columns, and he neglected the effect of sustained loading. He used the surfaces of failure representing strength capacity as shown in Figs. 1.2 and 1.3 to derive his equations. He used the surface of failure shown in Fig. 1.2 in terms of $1/P_u$, e_x and e_y to obtain Eq. (1):

$$\frac{1}{P_i} = \frac{1}{P_x} + \frac{1}{P_y} - \frac{1}{P_o} \tag{1.1}$$

where

P_i = Approximation of P_u

P_x and P_y = Load carrying capacities under compressive and uniaxial eccentricities e_x and e_y

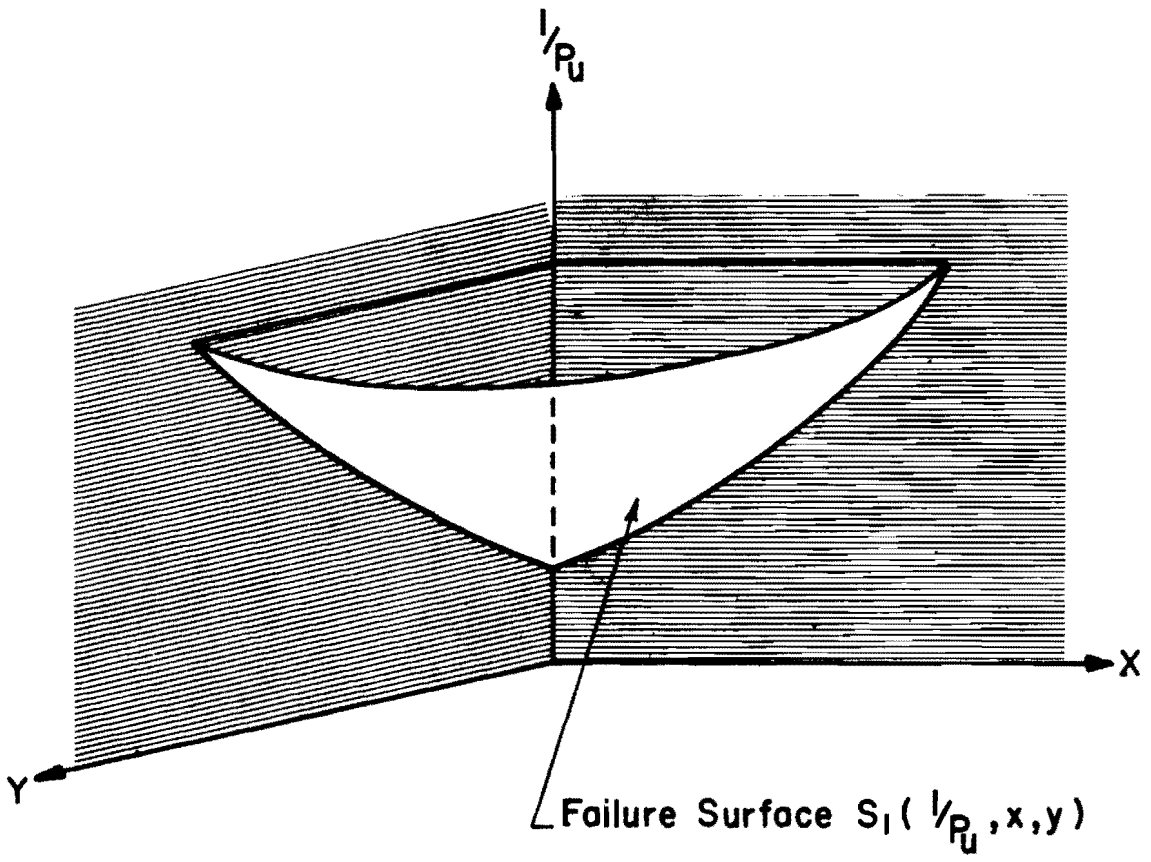

Fig. 1.2. Failure surface S_1.

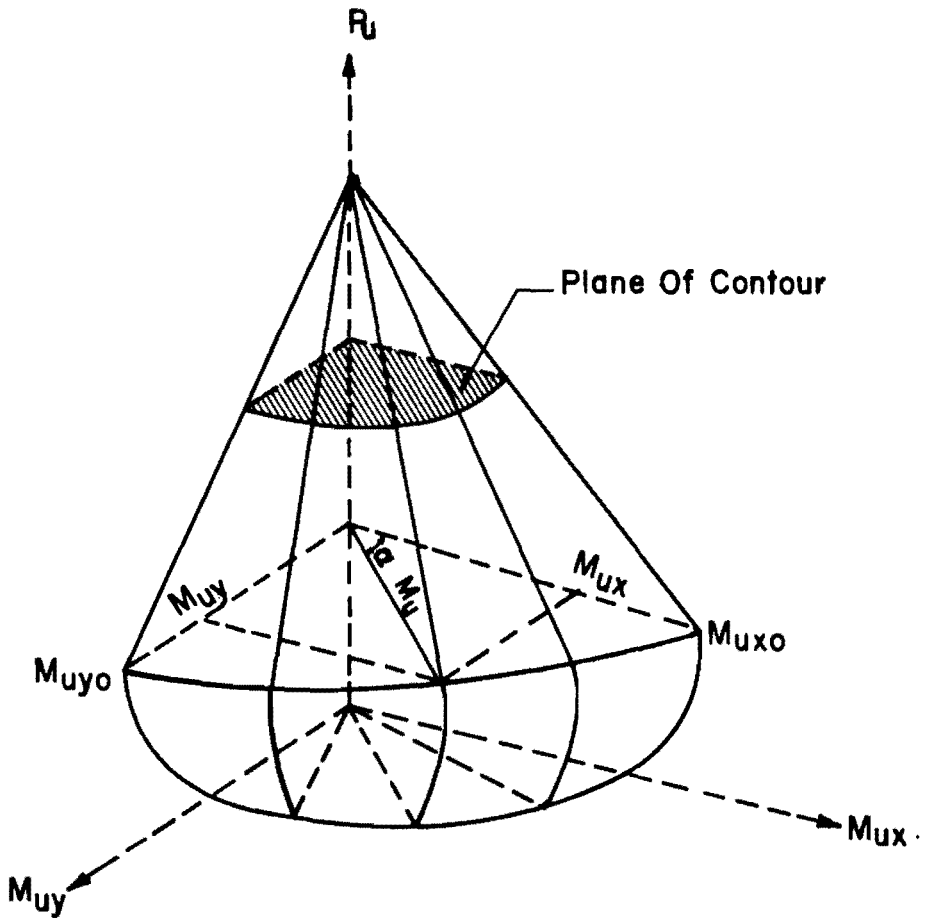

Failure Surface $S_2(P_u, M_{uy}, M_{ux})$

Fig. 1.3. Failure surface S_2.

P_o = Load carrying capacity under pure axial compression only

The surface of failure shown in Fig. 1.3 relates P, M_x and M_y. At any value of thrust, a "load contour" can be used to derive a moment interaction Eq. (1.2):

$$\left(\frac{M_x}{M_{xo}}\right)^{\alpha} + \left(\frac{M_y}{M_{yo}}\right)^{\beta} = 1.0 \qquad (1.2)$$

M_{xo} and M_{yo} = Moments due to uniaxial eccentricities x_o and y_o

M_x and M_y = Moments due to actual eccentricity

α and β = Exponent depending upon column dimension, amount and distribution of steel, stress-strain characteristic of steel and concrete, amount of concrete cover and arrangement and size of lateral ties or spiral

Bresler [6] found that with an average deviation of 3.3 percent the P_i predicted by Eq. (1.1) was in excellent agreement with test results while results from Eq. (1.2) provided good approximations with test results when values of α varied from 1.15 to 1.55.

Furlong [7] in 1961 reported an analytic study of ultimate strength capacity of square columns under biaxially eccentric loads using Whitney's equivalent rectangular stress distribution. He concluded that the square columns designed for biaxial bending could be checked by Eq. (1.3):

$$\left(\frac{m_x}{M_x}\right)^2 + \left(\frac{m_y}{M_y}\right)^2 \leq 1.0 \qquad (1.3)$$

m_x and m_y = Design moment in direction of major and minor axes

M_x and M_y = Moment capacity when P_u acts along the major and minor axes.

He also recommended that a reduction as large as 10 percent could be possible in cases where the ratio $(P_u - P_b)/P_b$ is less than 1.0 for the cross section.

Pannell [8,9] in 1963 proposed to transform rectangular sections into equivalent square columns by multiplying the rectangular section dimensions by the ratio M_{by}/M_{bx}, the ratio of balanced failure moments about major and minor axes at any specified ultimate thrust P_u. He developed Eq. (1.4) for transforming the actual moments to conform to the design surface

$$M_g = \frac{F\, M_y \sec \theta}{1 - N (\sin 2\theta)^2} \tag{1.4}$$

where

$$\theta = \tan^{-1} \frac{\varphi M_x}{M_y}$$

and

M_x, M_y = actual radial moment component with respect to the x and y axes.

φ = ratio M_{by}/M_{bx} for any load P.

F = A constant relating the failure surfaces of two identical columns except for depth of cover.

N = A deviation factor for the point of maximum deviation of the actual interaction surface from the idealized elliptic surfaces.

θ = Angle between x-axis and transformed failure plane.

M_g = The moment to be used in conjunction with the required failure load P.

Pannell [8,9] developed charts for values of N, F and φ. His method is designed for a cross section with equal steel distribution among four faces. He developed charts to select the best symmetrical multibar combination for any load system.

Ramamurthy [10] in 1966 proposed two equations to define approximately the shape of load contours that describe the capacity of square and rectangular columns. For constructing the interaction surface he proposed Eqs. (1.5) and (1.6) for a square column.

If $f_y \leq 40000$ psi

$$M_u = M_{uxo}\left(1 - 0.1\frac{\alpha}{45}\right) \tag{1.5}$$

and if $f_y = 60000$ psi

$$M_u = M_{uxo}\left(1 - 0.15\frac{\alpha}{45}\right) \tag{1.6}$$

For rectangular columns, if $f_y \leq 40000$ psi

$$M_u = M_{uxo}\left(1 - 0.1\frac{\alpha}{45}\right)\sqrt{\cos^2\beta + \frac{\sin^2\beta}{k^2}} \tag{1.7}$$

and if $f_y = 60000$ psi

$$M_u = M_{uxo}\left(1 - 0.15\frac{\alpha}{45}\right)\sqrt{\cos^2\beta + \frac{\sin^2\beta}{k^2}} \tag{1.8}$$

where

M_u = Ultimate radial moment

$$\sqrt{M_{ux}^2 + M_{uy}^2}$$

M_{ux} and M_{uy} = Ultimate moment about x and y axes.

M_{uxo} = Equivalent x-axis uniaxial moment of radial moment M_u.

α = $\tan^{-1} e_x/e_y$ = inclination of the line joining the load point to the centroid of the section to the y-axis.

β = Transformed equivalent angle of α; $\tan\beta = k\tan\alpha$.

k = Transformation factor.

Ramamurthy tested fifty columns of both square and rectangular shapes, and his equations gave good agreement with the test results. However, his columns were with small eccentricities. His resultant eccentricity e_r was always less than 20 percent of the section thickness. All of his specimens contained eight or more bars evenly distributed in each face.

Brettle and Warner [11,12] in 1968 described the concept of descretizing the column cross section into small elemental areas. By

superimposing a stress-strain curve upon the discrete element and by summing up the contribution of each individual elemental area, they were able to develop biaxial moment-thrust-curvature relationships. Results from columns tested by others have indicated reasonable agreement with predictions derived by their procedure.

Redwine [13] in 1974 developed a computer program entitled BIAM2, the foundation of which was similar to that reported by Farah and Huggins [14]. Redwine used a fourth order polynominal equation proposed by Farah and Huggins for the stress-strain relationship of concrete. He employed also their "closed form" equations to relate moments and biaxial curvature. He extended their study by integrating the curvatures to predict biaxial deformations. His analytical method agreed well with the few reported measurements of deformation under biaxial loading.

Fleming [15] compared the results from several methods for predicting the biaxial bending strength of cross sections, primarily for square or rectangular columns subjected to axial thrust and biaxial bending. The principal variable among proposed analysis methods has been the representation of stress and strain characteristics for concrete. Fleming [15]compared load contours of interaction surfaces generated by the various proposed methods. He concluded that the reciprocal thrust equation of Bresler, Eq. (1.1), offered the simplest accurate analytic expression for use in lieu of a computer program that employs discretized cross sections and test validates stress-strain functions for concrete.

1.3 Slenderness Effects Under Skew Bending

Strength design in accordance with ACI 318-71 (Eq. 10.5 of ACI 318-71) requires an analysis of secondary deformations in order to evaluate slenderness effects on columns. The approximate equations for estimating flexural stiffness for use in the moment magnification equation of ACI 318-71 do not take into account any combinations of biaxial effects from bending about a skewed axis. What moment magnifier should be used for skew bending? Should one use for the resultant moment, the larger of magnifiers determined independently for each principal axis? None of the

English language reports have included data regarding biaxial deformations of compression members.

1.4 Extension of Existing Knowledge

The analytical tools for predicting strength of cross sections appear to be available. Accurate strength estimates can be obtained either from closed form methods that employ the rectangular stress block for concrete or the more versatile discrete area representation proposed by Brettle - superimposing nonlinear stress-strain functions upon linear analysis then summing up the contribution of each individual element. Even Bresler's reciprocal thrust equation provides good results for effects from biaxial behavior, but it depends on good estimates of uniaxial behavior.

Columns can be designed on the basis of cross section strength only where the maximum amount of thrust and moment are available. Maximum moments in slender columns can be predicted for design only if stiffness characteristics can be predicted. The stiffness characteristics of concrete columns under biaxially eccentric thrust have not been measured or reported.

This report contains the test results from nine 5 X 9 in. rectangular specimens subjected to biaxially eccentric thrust. Three levels of thrust and three values of a nominal skew angle were used to produce failure of the specimen. Failure loads are compared with predictions derived from calculations based on the rectangular stress block for concrete strength and from more elaborate representations of concrete behavior at ultimate load. Stiffness data are reported from measurements of surface strain and from deformations taken in the direction of each principal axis.

CHAPTER II

TEST MEASUREMENTS

2.1 Specimens

Nine columns with a rectangular cross section 5 in. wide and 9 in. long were tested to failure. Nominal dimensions of each rectangular column designated RC-1 through RC-9 were identical and they were intended to represent 1/6 to 1/10 scale models of shapes required for bridge piers. The reinforcement details are shown in Fig. 2.1. Each column contained ten longitudinal 6 mm deformed bars ($\rho = 0.011$) and transverse ties of 13 gage wire spaced at 5 in. intervals.

In terms of squash load capacity P_o, thrust levels of 0.2 P_o, 0.4 P_o and 0.6 P_o were used. The safe value of P_o can be obtained analytically and for which no test is necessary. The uniaxial behavior of rectangular columns has been reported by a number of investigators [26, 27, 28] and there seems to be adequate confidence in analytic estimates of strength under uniaxial concentric thrust. For the points in the uniaxial thrust domain of an interaction surface, Panell [8] and Furlong [7] both observed that moment contours for strength differed very little from contours defined by the elliptical Eq. (1.3) unless thrust values were near P_{bal} for the cross section. Therefore, thrust ratios 0.2 P_o, 0.4 P_o and 0.6 P_o were selected for test loads in order to observe behavior below, near and above the probable values of P_{bal}.

Three groups of three columns each were made in order to be loaded for three different thrust levels and three nominal angles of eccentric thrusts. At each level of thrust the nominal skew bending angles were 22.5, 45 and 67.5 degrees, respectively, measured from the minor axis of the cross section. Specific thrust ratios and skew angles of each of the columns are given in Table 2.1.

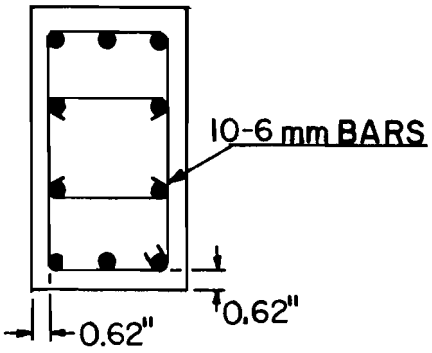

PLAN VIEW

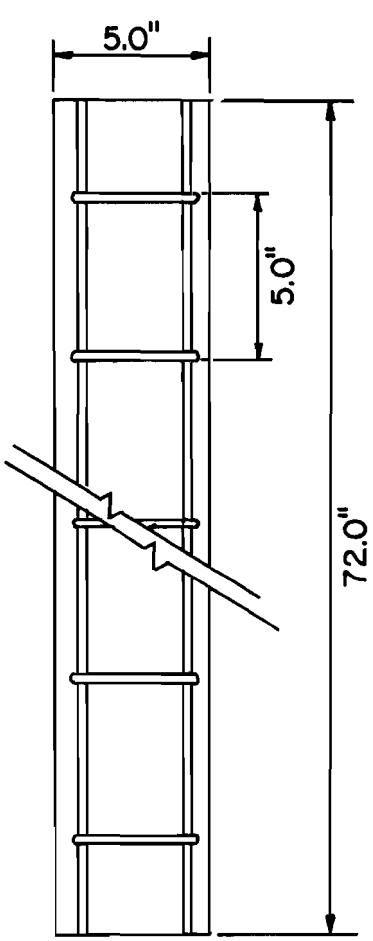

SIDE VIEW

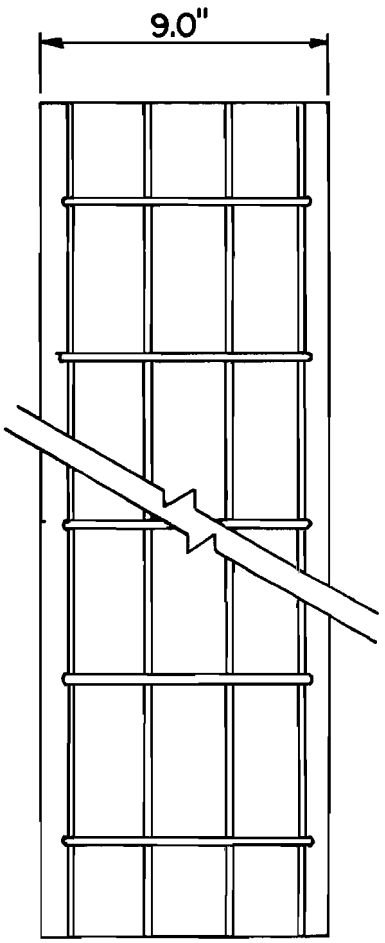

ELEVATION

Fig. 2.1. Test specimen.

TABLE 2.1. TESTING SEQUENCE

Specimen	Thrust Level	Nominal Skew Angle Degrees	Moment Arm in.	
			Weak Axis	Strong Axis
RC-1	0.6 P_o	67.5	24.15	10.0
RC-2	0.6 P_o	45.0	24.15	24.15
RC-3	0.4 P_o	45.0	24.15	24.15
RC-4	0.6 P_o	22.5	10.0	24.15
RC-5	0.4 P_o	67.5	24.15	10.0
RC-6	0.2 P_o	67.5	24.15	10.0
RC-7	0.2 P_o	45.0	24.15	24.15
RC-8	0.2 P_o	22.5	10.0	24.15
RC-9	0.4 P_o	22.5	10.0	24.15

2.2 Materials

A mix of Class A concrete was designed according to the Texas Highway Department's specifications [21]. Concrete was mixed in an 11 cu. ft. capacity rotary mixer. A total volume of 6 cu. ft. of concrete mix was used to cast ten standard test cylinders and one test column of 5 in. x 9 in. in cross section and 72 in. long. All specimens were cast vertically with concrete placed from the top of the metal form. The form was vibrated externally. After removing the casting form the test specimen and cylinders were kept covered under plastic sheets in a moist condition for seven days.

The concrete mix was designed for a cylinder strength of 4000 psi. Quantities of different ingredients used for the mix are shown in Table 2.2.

The measured 28 day strength of cylinders varied between 4300 psi and 5200 psi. The cylinder strength of all nine rectangular columns are shown in Table 2.3. The values shown in Table 2.3 are the average values of total ten cylinders. Half of the cylinders were tested before starting the new test and the rest were tested after the test was over.

TABLE 2.2 CONCRETE MIX

Ingredients	6 cu. ft. Mix
Cement Type I	125.5 lbs.
Coarse Aggregate	424.0 lbs.
Sand	264.0 lbs.
Water	37.5 lbs.
Septair	40.0 cc

TABLE 2.3 COMPRESSIVE STRENGTH

Specimen	28-day* Cylinder Strength in. psi	Specimen	28-day* Cylinder Strength in. psi
RC-1	4886	RC-6	4425
RC-2	4871	RC-7	4350
RC-3	5210	RC-8	4446
RC-4	5181	RC-9	4700
RC-5	5012		

*Average of ten cylinders

Except for RC-3, RC-4, and RC-7 the variation of strength is within 300 psi of 4720 psi. The average strength of all nine specimens was 4788 psi which is about 19.7 percent higher than the nominal mix value.

Deformed steel bars of 6 mm diameter were used as longitudinal reinforcing bars and 13 gage wires were used for ties with vertical spacing of 5 in. on centers. A typical stress-strain curve for the 6 mm deformed bar is shown in Fig. 2.2. There was a total of eight bars tested. The average area of a bar was 0.049 in. square using 0.283565 lb./in.^{3} steel density as shown in Table 2.4. The average yield stress of the bar tested is 66.5 ksi with modulus of elasticity of 30,000,000 psi.

2.3 Loading System and Measurement

The magnitude of each load was measured with load cells, hydraulic pressure dial and with hydraulic pressure transducers in each loading system.

Three load cells, each of about 100 kips capacity, were used in parallel beneath the test specimen to measure the nominal axial load,

TABLE 2.4 REINFORCEMENT TESTS RESULTS*

Specimen	Length in.	Weight lbs.	Volume in.^{3}	Area in.^{2}	Yield Stress ksi	Ultimate Stress ksi
RC-1 A	45.0	0.62	2.194	0.04875	65.6	94.56
RC-1 B	44.948	0.62	2.199	0.04887	65.44	93.56
RC-4	37.563	0.51	1.799	0.04788	66.327	95.92
RC-7	37.625	0.51	1.799	0.04780	67.347	95.918
RC-9	37.563	0.51	1.799	0.04788	65.306	93.877
C-8**	37.625	0.51	1.799	0.04780	66.327	91.837

*Density of Steel = 0.283565 lb./in.^{3}

**Along with nine rectangular columns, fifteen partial circle columns were tested [16].

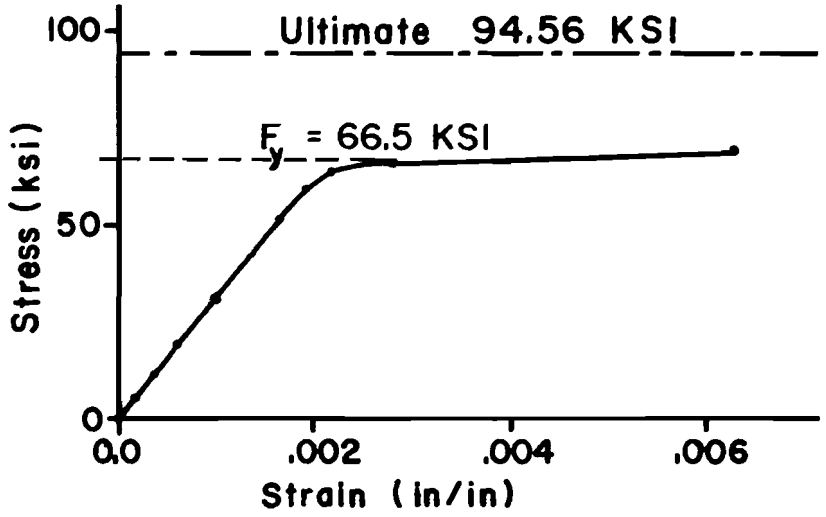

Fig. 2.2. Stress-strain curve for 6mm ϕ bar.

and one load cell each of about 10 kips capacity was used to measure each of the side moment loads. The loading technique that was used is shown schematically in Fig. 2.3.

Axial load was applied through one big central ram and an electrically operated hydraulic pump while moment load was applied through the two small rams, one on the west and the other on the south side pressured by a manually operated hydraulic pump. In the beginning of each test only axial load P_c was applied in stages of approximately 10 to 20 kips, during which no moment load was applied. Once the desired thrust level had been achieved, side arm loads P_s and P_w were applied in stages of approximately 0.25 to 0.50 kips until the failure of column occurred. At flexural load increments the magnitude of P_c was adjusted in order to keep the total thrust, $P_c + P_w + P_s$ constant throughout each test. During each load stage the side loads P_s and P_w were kept equal in magnitude because each was actuated from the same pump. Due to differences in the cross-sectional area of the loading rams a little difference in load cell readings was observed through VIDAR measuring system. The difference between load cell measurements was maximum of 150 lbs. when the average load was 9045 lbs.

The loading arm distances "a" and "b" were changed, as shown in Table 2.1 to control the nominal skew angle of loading. Thus, the skew angle of load α can be found by either Eq. (2.1) or Eq. (2.2).

$$\alpha = \tan^{-1} \frac{P_w \times a}{P_s \times b} \tag{2.1}$$

since $P_w = P_s$

$$\alpha = \tan^{-1} \frac{a}{b} \tag{2.2}$$

Steel beams were attached to a fabricated plate steel loading head to facilitate the application of eccentric loading, P_s and P_w, in both principal axes. The loading diagram is shown in Fig. 2.4 (reproduced from Ref. [6]).

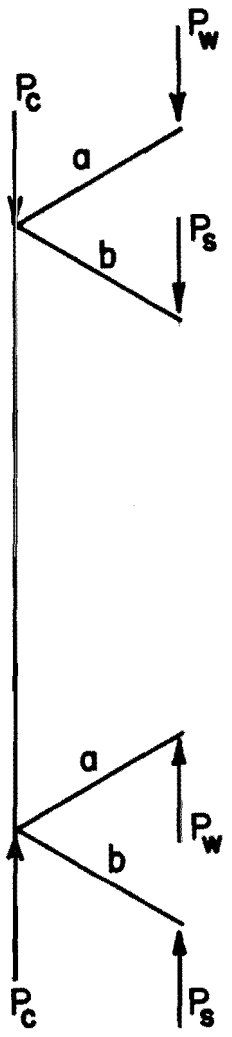

Fig. 2.3. Schematic arrangement of loading technique.

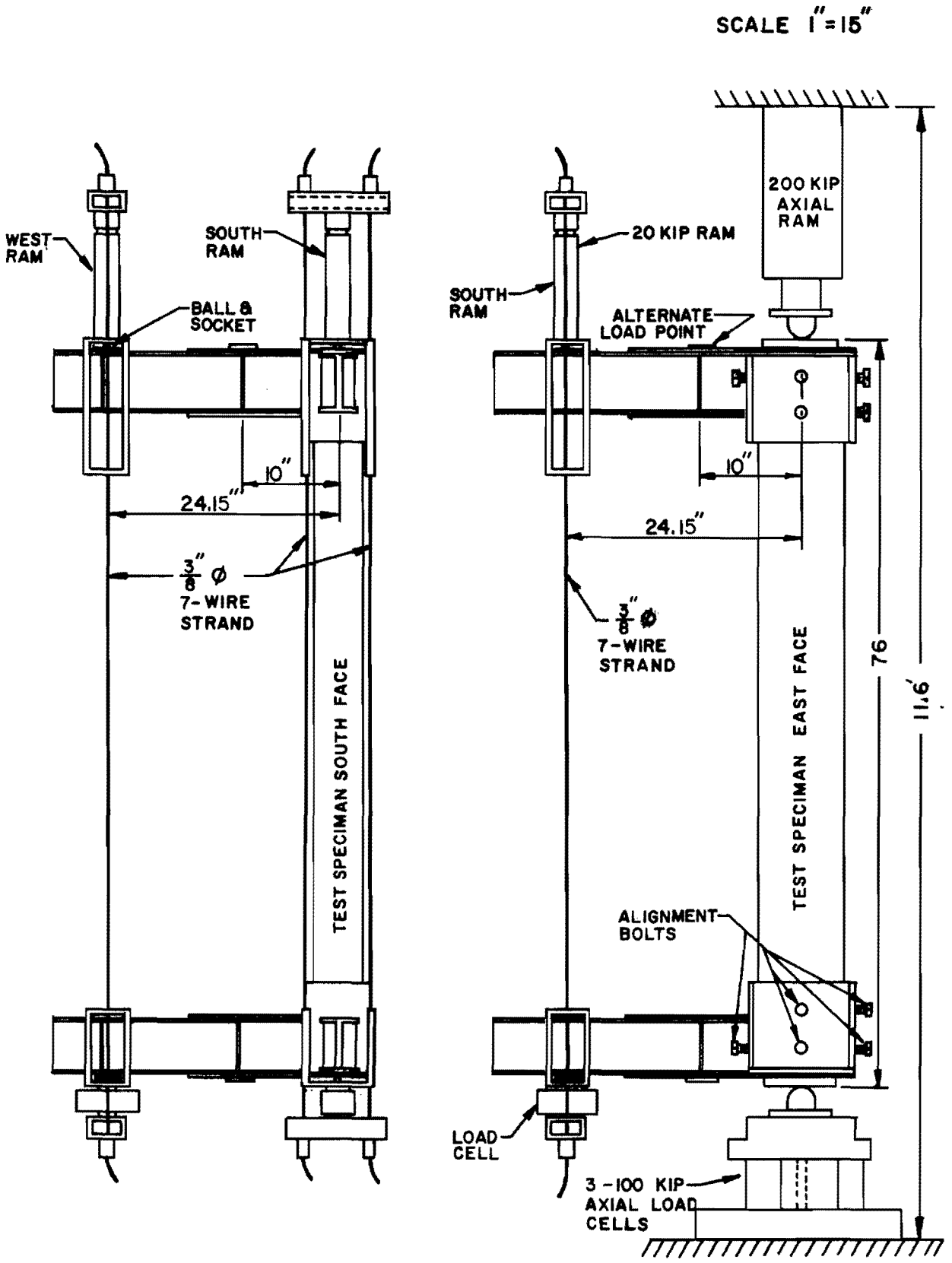

Fig. 2.4. Diagram of loading frame.

2.4 Deformation Measurement

Two different types of displacement data, deflection and surface strain measurements were taken for each stage of loading during each test. Most displacement measurements were obtained with linear potentiometers in order to observe an electrical signal for remote recording. A dial indicator used for weak axis deformation was used principally for control during the test.

The test column was marked off longitudinally into five sections, each 6 in. long. Potentiometers were mounted opposite each face of the column at the end of steel frames as shown in Figs. 2.5 and 2.6. A total of twenty measuring stations were used to define the condition of surface strain along the central 30 in. of each specimen. The technique used to measure surface strain was similar to that used by Chang, Breen, Furlong, Green, et al. [17,18,19,20], except that for the present study, biaxial strains were to be measured.

Lateral deflections were measured at the middle of each strain gage station in the directions of both the weak and the strong axes of the column cross section. For weak axis deflection, dial gages with a 2 in. travel were also mounted at mid-depth of the test column and 8 in. away from both the north face and the south face of the test specimen. Once the side load was applied (as mentioned in Section 2.3) at the end of each further load stage a graph of applied moment load vs. weak axis dial gage reading, i.e., weak axis deflection, was prepared. The graphs for different thrust levels are shown in Figs. 2.7, 2.8, and 2.9. Each graph was helpful as a control for selection of load increments in each of the test procedures. As the slope of the graph decreased, load increments also were decreased. When the slope reached zero, the loading could be terminated before an explosive type failure damaged the measuring equipment. In spite of the precautions, some loss of linear potentiometers was unavoidable when sudden failure did occur.

All data from the potentiometers were recorded through a VIDAR unit on magnetic tape as well as a printed teletype page. The VIDAR recording unit is a part of an electronic data acquisition system. As a

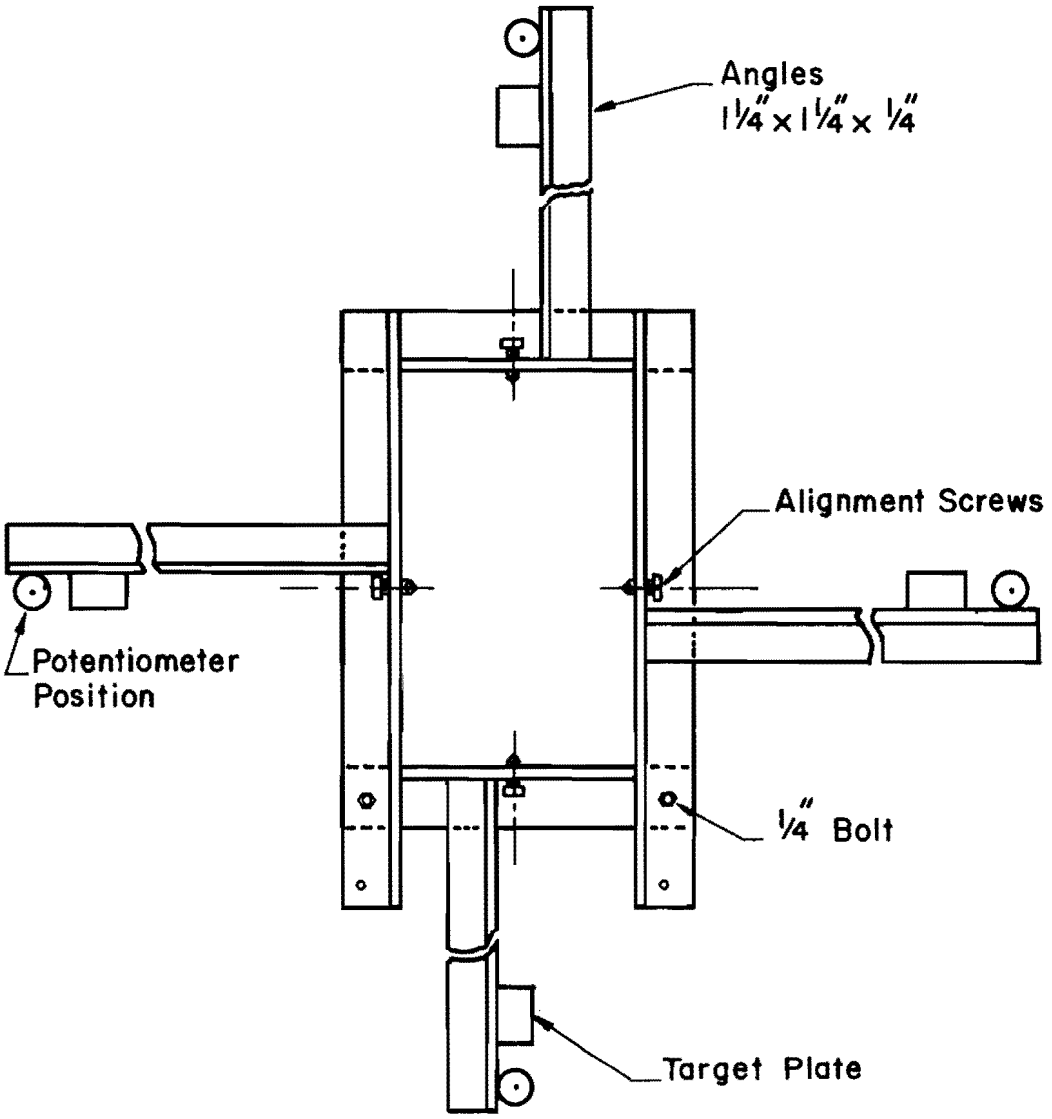

Steel Frame For Positioning Linear Potentiometer

Fig. 2.5. Steel frame for positioning linear potentiometer.

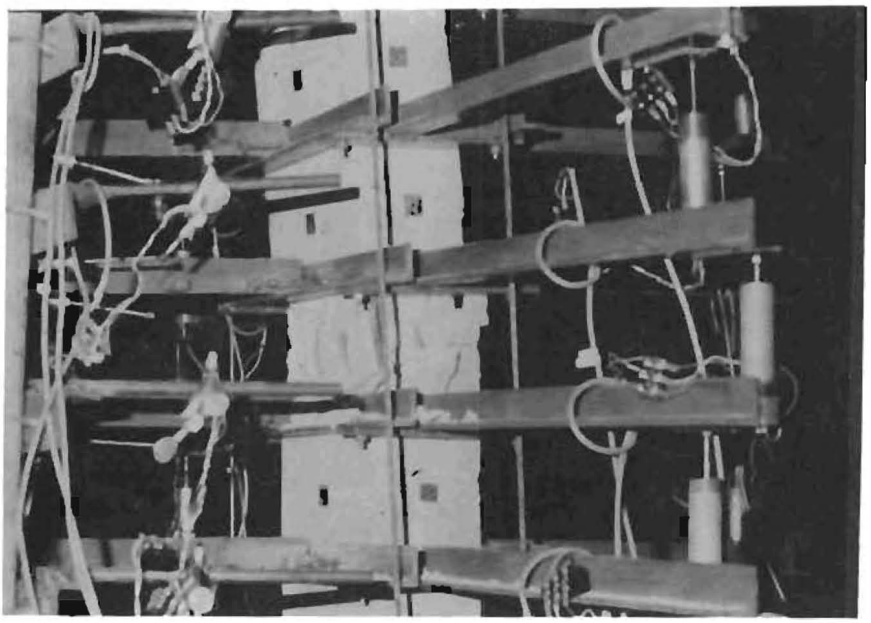

Fig. 2.6. Steel frame and potentiometers in position.

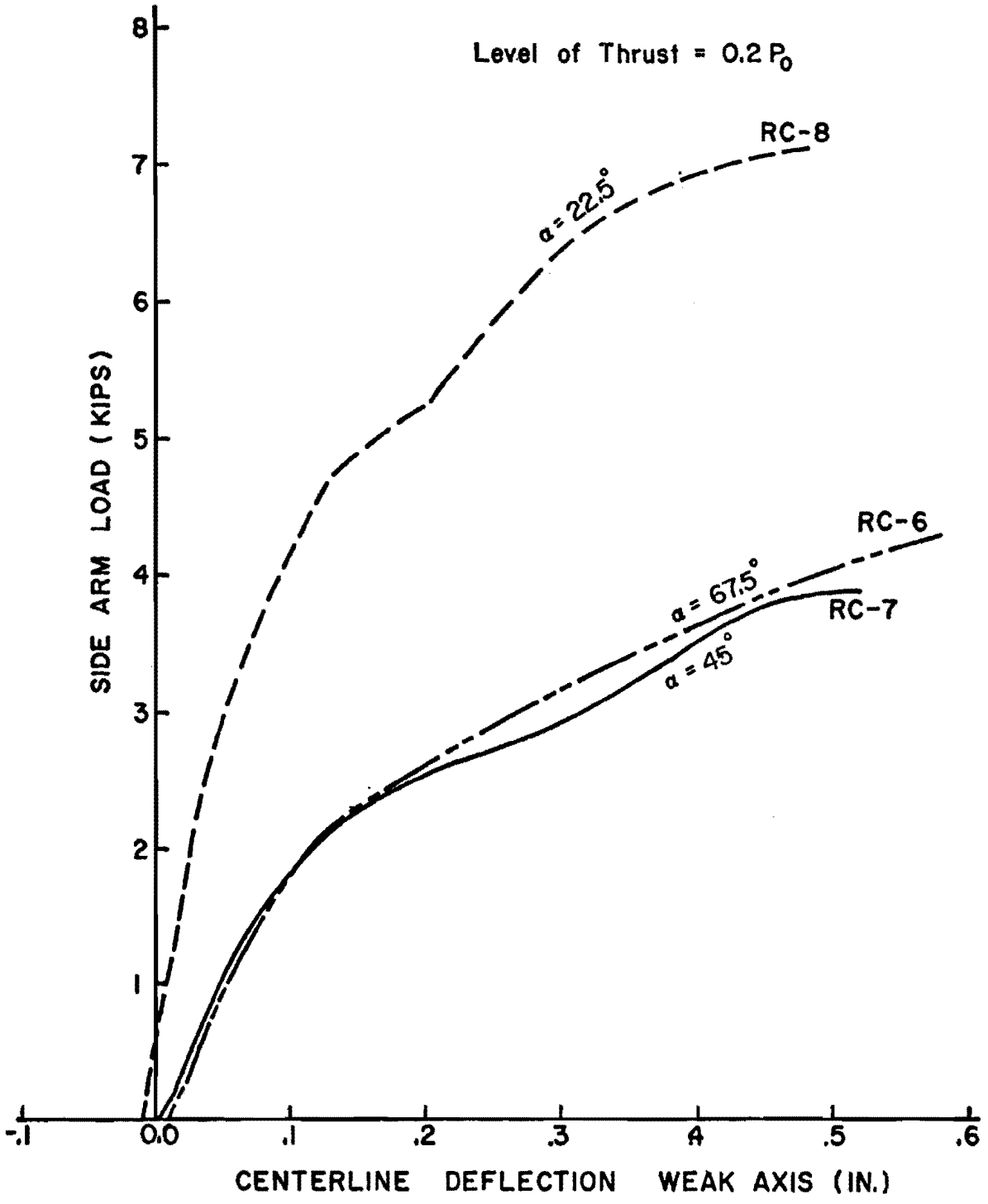

Fig. 2.7. Deflection curves - thrust level $0.2P_o$.

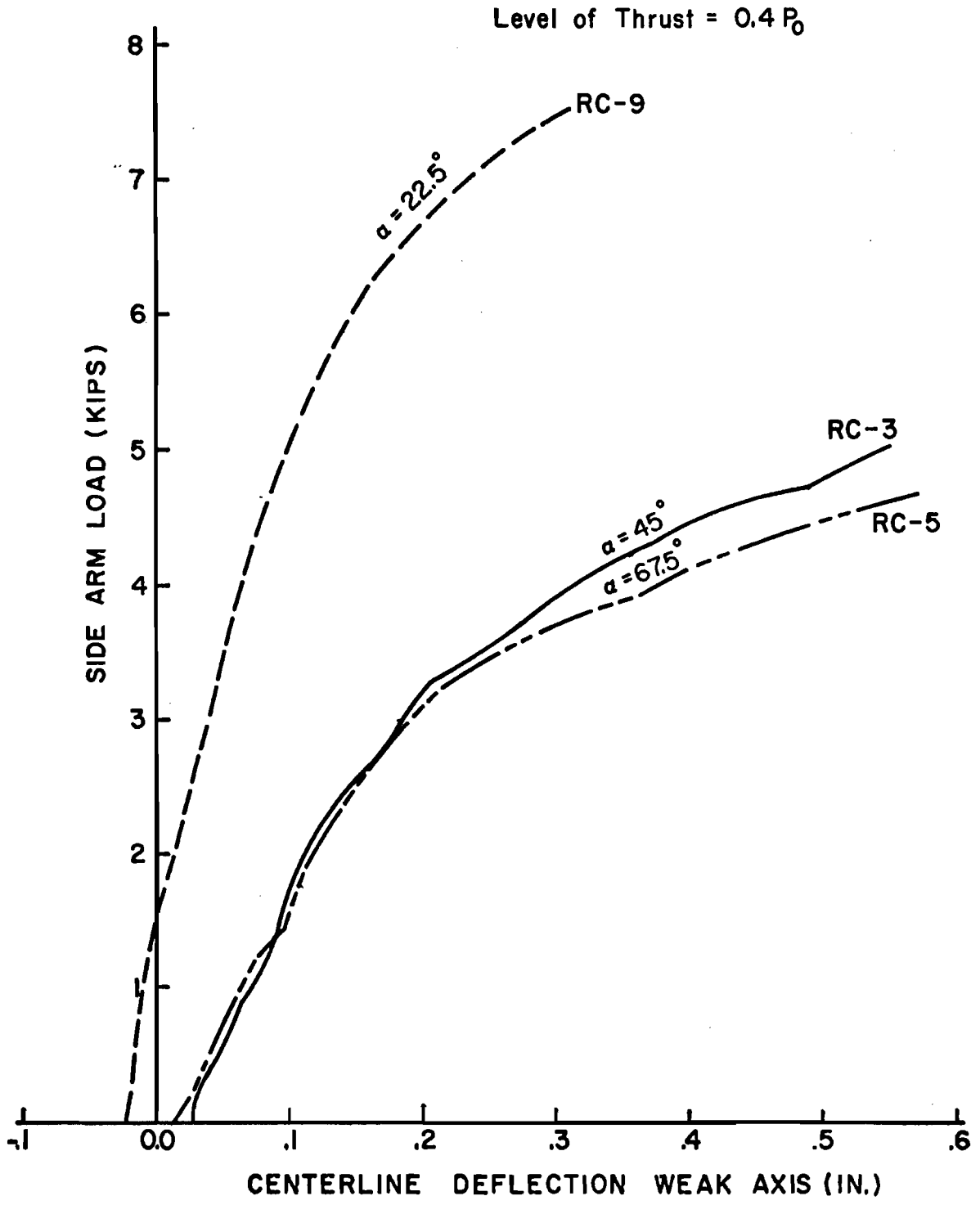

Fig. 2.8. Deflection curves - thrust level $0.4P_o$.

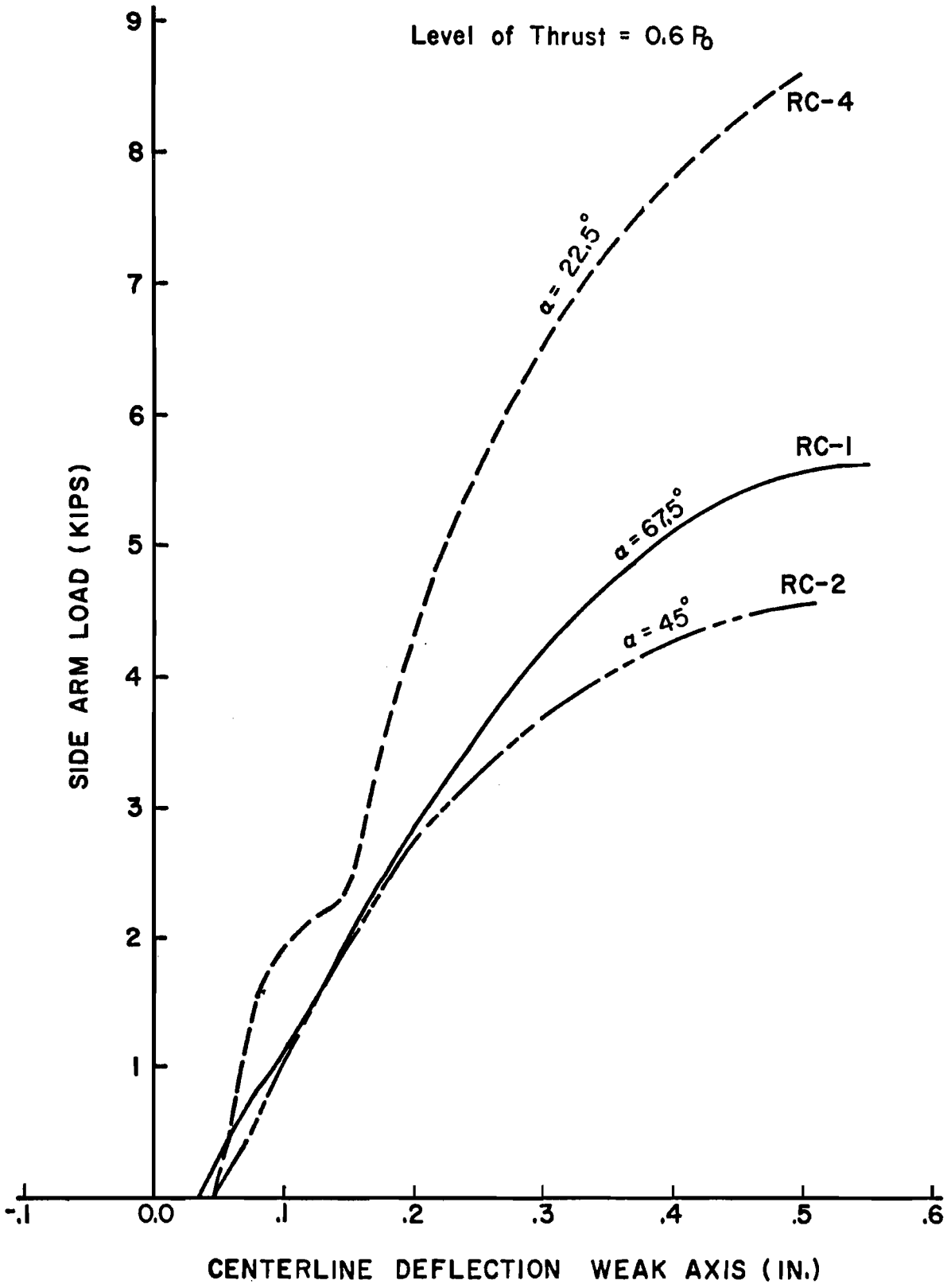

Fig. 2.9. Deflection curves - thrust level $0.6P_o$.

cross check against the remote data acquisition system, the dial gage readings of weak axis deflection were compared with the deflection readings obtained from the VIDAR. Insignificant differences were observed as shown in Table 2.5. The data of Table 2.5 are representative for all of the tests that were made.

A complete setup of a test with all instruments in place is shown in Fig. 2.10. Details regarding preparation of each test specimen, the specific test procedure and interpretation of data accumulated are described in detail in Ref. [16].

TABLE 2.5 COMPARISON OF DIAL GAGE AND VIDAR READINGS TEST SPECIMEN RC-5

	Moment Load kips	Weak Axis Deflection	
		Dial Gage	VIDAR
1	0.0	0.016	0.015
2	0.32	0.032	0.029
3	0.51	0.042	0.039
4	1.24	0.075	0.073
5	1.41	0.091	0.085
6	1.91	0.112	0.109
7	2.4	0.139	0.135
8	2.9	0.181	0.173
9	3.39	0.239	0.229
10	3.51	0.262	0.256
11	3.63	0.387	0.276
12	3.75	0.308	0.301
13	3.85	0.331	0.323
14	3.90	0.362	0.353
15	4.09	0.388	0.378
16	4.21	0.417	0.405
17	4.33	0.448	0.436
18	4.44	0.484	0.471
19	4.55	0.526	0.514
20	4.68	0.572	0.554

Fig. 2.10. Complete set of test with all instruments in place.

CHAPTER III

TEST RESULTS

3.1 General

The data concerning deflection, surface strain and load were recorded on magnetic tape through a scanner and a VIDAR electronic data acquisition system. The scanner can be used to scan 240 channels. It connects to the VIDAR recorder through a single cable permitting easy access to remote test locations. These recorded data were then reduced to engineering units of inches and kips with the help of a standard data reduction computer program associated with the data acquisition system. Another data reduction program that was written by Green [16] was used to reduce the engineering data to prepare tabulations of axial load, applied moments, skew bending angles, measured deflection, corner strain, steel stresses, second order moments, neutral axis locations and curvatures. The specific details of logic used for data reduction can be found in Ref. 16.

This chapter deals with the strength and stiffness analysis of all nine rectangular columns that were tested.

All the columns were vertically cast. Listed below are the positions of failure for all nine specimens. All the positions are noted relative to the casting position.

TABLE 3.1. LOCATION OF FAILURE

Specimen	Load Level	Position of Failure
RC-1	$0.6P_o$	midheight
RC-2	$0.6P_o$	6 in. above midheight
RC-3	$0.4P_o$	midheight
RC-4	$0.6P_o$	6 in. below midheight
RC-5	$0.4P_o$	6 in. above midheight
RC-6	$0.2P_o$	midheight
RC-7	$0.2P_o$	3 in. above midheight
RC-8	$0.2P_o$	midheight
RC-9	$0.4P_o$	12 in. above midheight

3.2 Maximum Moments

In order to calculate the maximum moments that actually existed near midheight of the specimen, it was necessary to include (1) the effect of the movement of the column head during application of axial load, (2) the effect of initial end eccentricity corresponding to the actual position of the axial load ram and (3) the effect of change in end eccentricity after moment forces were applied. Each of the effects was treated by Green, but significant details are repeated in the following paragraphs.

During the application of axial load some lateral movement of the column occurred. The movement was less significant after the axial load level had been reached and skew bending forces were being applied. The displacement of the column during axial load application had to be taken into account in the determination of the effective deflection at each station along the length of columns. Additional measured lateral deflections were included in calculations of the secondary moments.

The apparent end moment required a correction from readings of deflection because of rotations of the loading head. This correction was made as described for specimen RC-2 as follows.

In the weak axis direction the measurements of deflected shape of Column RC-2, due to the application of axial load at each load stage are shown in Fig. 3.1. The deflection of specimen RC-2 is representative of all nine columns.

The deflection readings at each load stage were plotted along the length of the column as shown in Fig. 3.1. A curve passing through these plotted points was drawn and extended longitudinally to meet the head position of columns which were 36 in. above and below the midheight deflection station of each specimen. As seen from Fig. 3.1, the bottom and top position of bearings are not in the same vertical location. Some movement of the loading heads occurred during the application of axial load. A correction in the reading of deflection was necessary due to the movement of heads. The broken line joining the top and bottom positions of loading heads on Fig. 3.1 was defined as the initial position of the column.

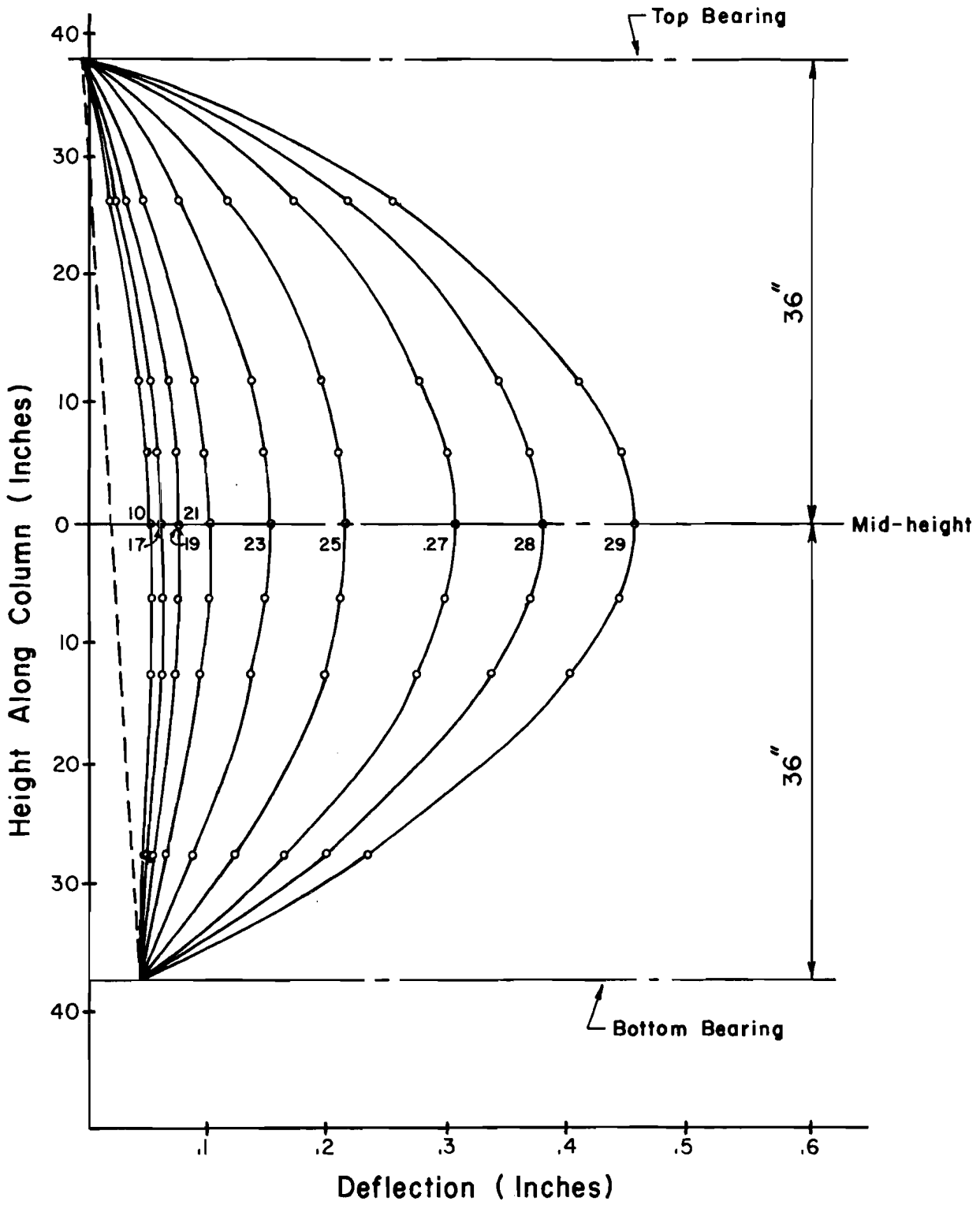

Fig. 3.1. RC-2 weak axis deflection.

The actual reading of deflection at each station was corrected then for this new position as shown in Fig. 3.2. Since the rounded end bearings could not resist moments, the initial position line had to represent the line of action of column force between ends of the column. The line of action was not vertical generally, and its use as a deflection reference automatically incorporated into the moment equation the resultant thrust, including any horizontal as well as vertical reaction.

An initial eccentricity existed at the ends of each specimen due to inevitable misalignment of the axial load ram from the axial centroid of the specimen. The initial end eccentricity was estimated to be not more than 0.15 in. in any case, but the effect of it on the secondary moment was significant. The specimen and loading heads were aligned to conform with transit sight lines in both the major and minor axis directions. It was physically impossible to align perfectly the force system that was used, and since secondary moment corrections were known to be necessary as a part of the data interpretation, "perfect" alignment was not considered to be feasible. The magnitude of initial eccentricity was estimated from the measured corrected deflections before moment loads were applied.

Estimates of the axial ram eccentricity were made with the aid of elastic beam column theory [22]. Under axial load alone the entire cross section was in compression. The eccentricity e_i can be calculated using Eq. (3.1).

$$e_i = \frac{\Delta_{ci} E_c I_T}{P \times L^2} \left[\frac{(u^2 \cos u)}{2(1 - \cos u)}\right] \tag{3.1}$$

where

e_i = axial ram eccentricity in inches

Δ_{ci} = corrected centerline deflection in inches

E_c = modulus of elasticity of concrete in psi

I_T = moment of inertia of transformed section

L = length of column in inches

P = axial thrust in pounds

$u = L/2 \sqrt{P/E_c I_T}$

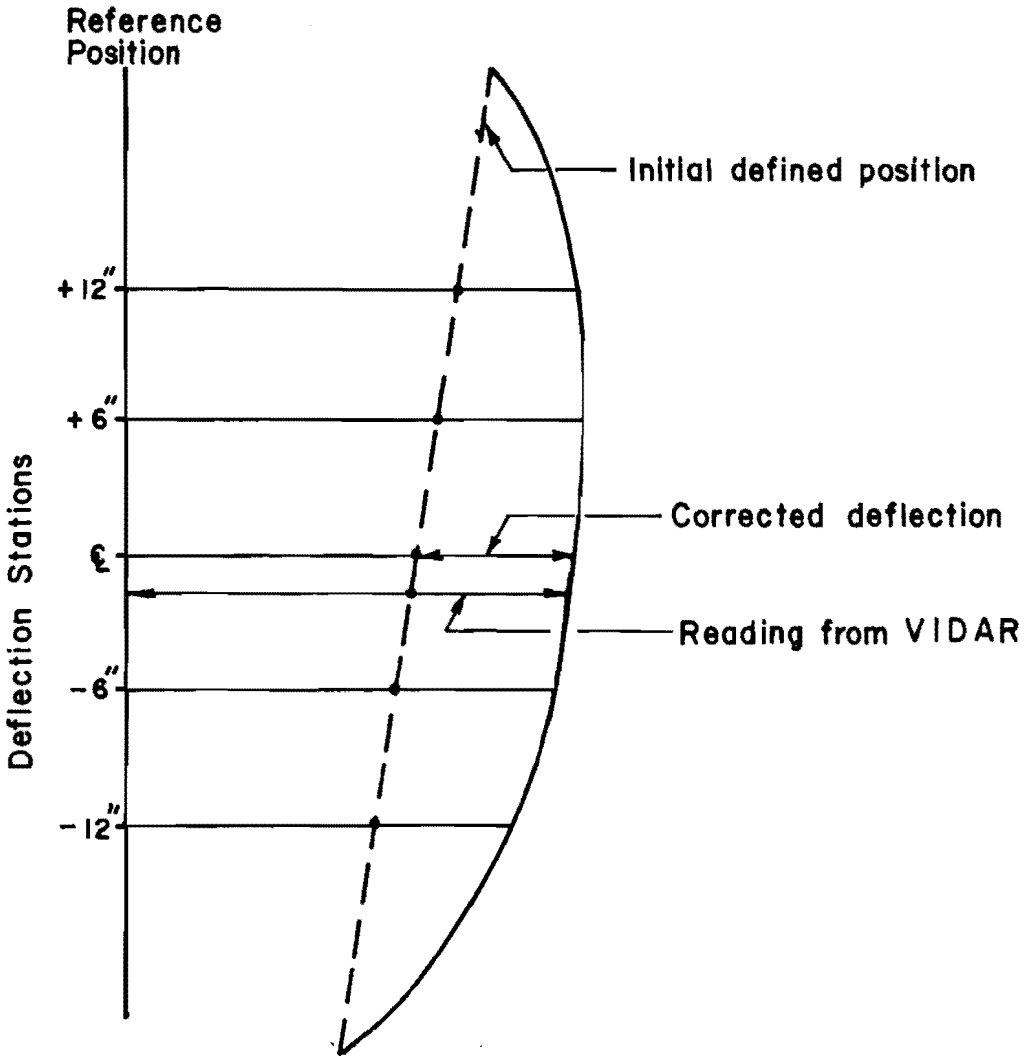

Fig. 3.2. Deflection readings correction.

Values of e_i were calculated for the corresponding load stages just before eccentric moment arms were first loaded. Results from the calculation of e_i are recorded in Table 3.2.

As the loading progressed the effective end eccentricity changed as the bearing rotated. Spherical balls were used at both ends of the column as end bearings, although the "spherical" balls were flattened somewhat against loading plates. The flatness of the bearings contributed to the change in the true end eccentricity.

The rotation of flattened end bearings created a change in end eccentricity for each axis. The changes were calculated assuming that the deflected shape of the column was a half cycle of a sine wave (Fig. 3.3). The change in end eccentricity, e_c can be calculated by Eq. (3.2).

$$e_c = R\frac{\pi}{\ell}\Delta_c \tag{3.2}$$

where

R = radius of ball in inches

ℓ = length of column in inches

Δ_c = corrected central line deflection at the ultimate load in inches

The derivation of Eq. (3.2) in more detail is explained by Green [16]. The recommended values of R were 18 in. and the length of the column, ℓ was 76 in. [16].

The above correction for the change in end eccentricity is shown schematically in Fig. 3.4.

The total thrust, P_T, is simply the sum of ram loads as per Eq. (3.3):

$$P_T = P_c + P_w + P_s \tag{3.3}$$

where

P_c = axial thrust in kips

P_w = load on weak axis moment arm in kips

P_s = load on strong axis moment arm in kips

TABLE 3.2. INITIAL ECCENTRICITIES

Specimen	Thrust Level P/P_o	P kips	E_c ksi	Axis	I_T $in.^4$	$\sqrt{\frac{P}{E_c I_T}}$	u	cos u	Δ_{ci} in.	e_i in.
RC-1	0.6	115	4027	Weak	102.69	0.0166	0.6311	0.8073	0.0060	0.0252
				Strong	336.83	0.0092	0.3484	0.9398	0.00090	0.01415
RC-2	0.6	109	4021	Weak	102.70	0.0162	0.6167	0.8157	0.0091	0.0406
				Strong	336.88	0.0090	0.3405	0.9425	-0.0043	-0.0706
RC-3	0.4	95	4159	Weak	102.41	0.0149	0.5645	0.8448	0.0089	-0.04889
				Strong	335.78	0.0082	0.31170	0.9518	-0.00055	-0.01088
RC-4	0.6	135	4147	Weak	102.43	0.0177	0.6744	0.7810	0.0365	0.13019
				Strong	335.87	0.0098	0.3724	0.9314	0.0061	0.08287
RC-5	0.4	88	4079	Weak	102.58	0.0145	0.5496	0.8526	0.02209	0.12787
				Strong	336.41	0.0080	0.3034	0.9542	-0.0051	-0.10683
RC-6	0.2	33	3833	Weak	103.14	0.0091	0.3466	0.9405	0.0075	0.11901
				Strong	338.5	0.0050	0.1914	0.9817	-0.0035	-0.19216
RC-7	0.2	40	3800	Weak	103.22	0.0101	0.3852	0.9266	0.0056	0.07174
				Strong	338.8	0.0056	0.2128	0.9774	-0.0027	-0.12111
RC-8	0.2	40	3842	Weak	103.12	0.0096	0.3649	0.9341	-0.0027	-0.0383
				Strong	338.42	0.0058	0.2220	0.9754	-0.004	-0.1588
RC-9	0.4	93	3950	Weak	102.86	0.0150	0.5728	0.8403	-0.0141	-0.07468
				Strong	337.47	0.0083	0.3162	0.9503	0.0066	0.12646

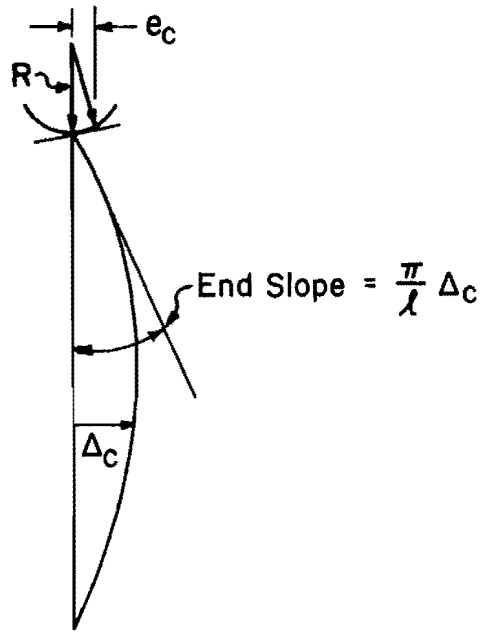

Fig. 3.3. Representation of deflected shape as sine wave.

The final moments at midheight of each column for each axis can be calculated using the following equations:

$$M_s = b \times P_s + P_T \times \Delta_{cs} - P_T \times e_{cs} + P_c \times e_{is} \qquad (3.4)$$

$$M_w = a \times P_w + P_T \times \Delta_{cw} - P_T \times e_{cw} + P_c \times e_{iw} \qquad (3.5)$$

where

M_w, M_s = final effective moment for weak and strong axis

a, b = moment arm distances for weak and strong axis

Δ_{cw}, Δ_{cs} = as defined in Eq. (3.2)

e_{cw}, e_{cs} = as defined in Eq. (3.2)

e_{iw}, e_{is} = as defined in Eq. (3.1)

These equations were then used to calculate moments at each load stage using the computer program. The final calculated moment values are tabulated in Table 3.3. Table 3.3 is the tabulation summary for basic input and observed load quantities for all nine specimens.

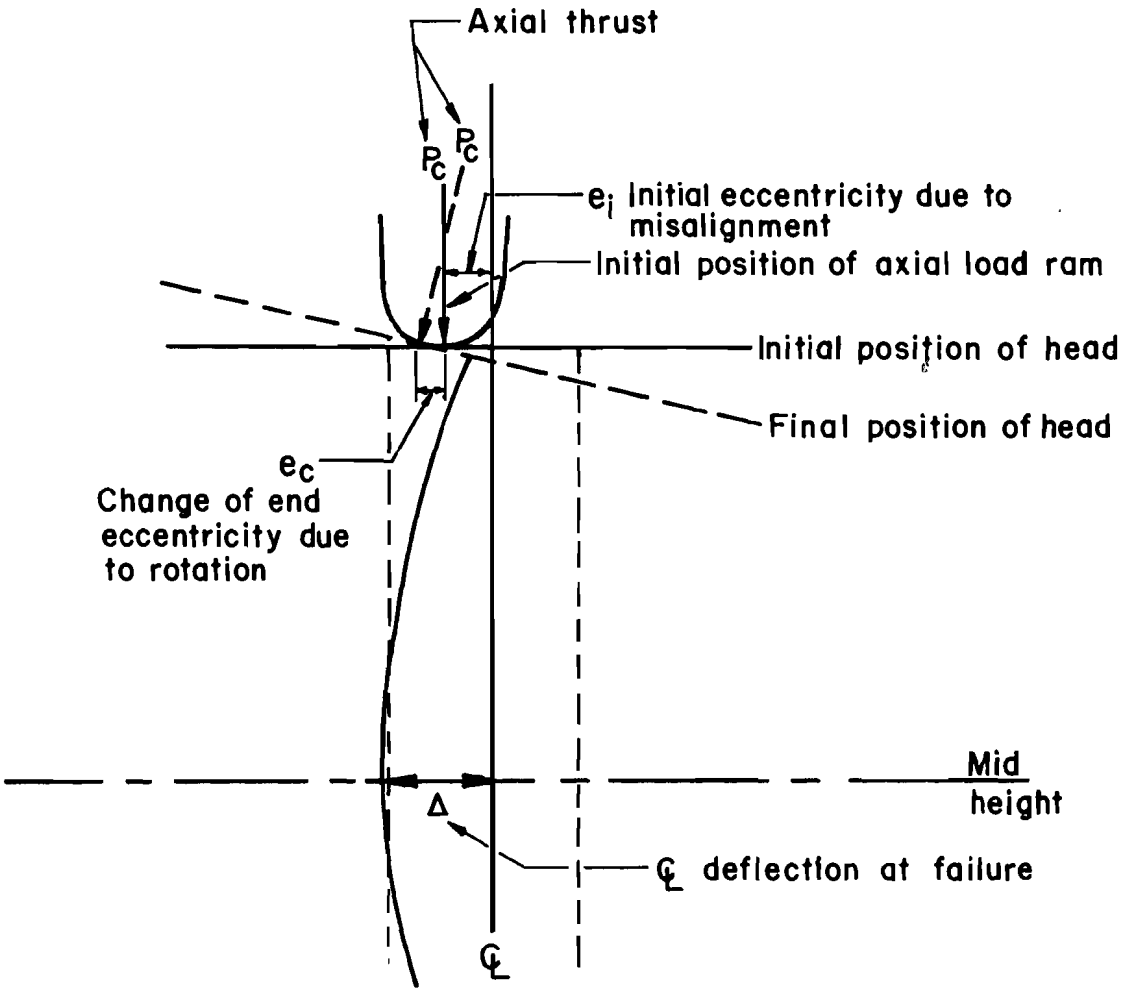

Fig. 3.4. Change in end eccentricity.

TABLE 3.3. SUMMARY OF TEST RESULTS

Specimen	f'_c psi	Nominal Skew Angle of Loading Degree	Actual Skew Angle of Loading Degree	P_o kips	Ultimate Load Stage Number	P_{test} kips	Nominal Thrust Level P/P_o	Actual Thrust Level Achieved P_u/P_o	Load Stage at First Crack	M_{CR} kips - in.		M_{test} kips - in.		ϵ_c Comp. Strain in./in.	ϵ_t Tensile Strain in./in.
										Weak	Strong	Weak	Strong		
RC-1	4886	67.5	65.12	219.0	30	119.2	0.6	0.544	23	87.91	40.03	184.46	70.35	0.00374	-0.00369
RC-2	4871	45.0	41.0	218.4	40	120.3	0.6	0.551	29	140.63	113.0	154.99	124.0	0.00431	-0.00420
RC-3	5210	45.0	38.4	231.4	33	95.1	0.4	0.411	21	97.78	81.61	160.69	131.87	0.00418	-0.00470
RC-4	5181	22.5	19.8	230.3	54	128.9	0.6	0.556	31	79.74	126.03	132.32	227.83	0.00360	-0.00525
RC-5	5012	67.5	61.3	223.8	40	87.1	0.4	0.389	81	95.11	33.72	151.50	52.77	0.00410	-0.00372
RC-6	4425	67.5	63.2	201.4	39	53.5	0.2	0.266	16	58.90	24.57	135.68	52.33	0.00185	-0.00451
RC-7	4350	45.0	42.3	198.5	33	38.9	0.2	0.196	17	63.28	57.98	116.44	104.94	0.00461	-0.0109
RC-8	4446	22.5	20.6	202.2	38	40.4	0.2	0.200	19	33.69	81.06	86.44	190.38	0.00476	-0.00860
RC-9	4700	22.5	18.9	211.9	26	85.05	0.4	0.401	16	50.02	116.91	96.41	209.31	0.00424	-0.00526

3.3 Analytic Estimates of Capacity

A rectangular stress block was used to represent concrete stress-strain characteristics foranalytic estimates of cross section strength. Estimated moment capacity for each nominal skew angle and thrust were compared with the measured strength of test columns. The analytic load capacity (squash load capacity P_o) was estimated using Eq. (3.5a)

$$P_o = 0.85f'_c + A_s F_y \qquad (3.5a)$$

Using the rectangular stress block, the points on interaction diagrams adequate to define an interaction surface were calculated. A computer program was developed to save time in hand calculation for finding the points on the interaction surface. Interaction diagrams were determined for each axis of bending and for all values of the concrete strengths shown in Table 2.4 (f'_c from 4.35 to 5.10 ksi). A sample interaction diagram for maximum concrete strength and minimum concrete strength for both strong and weak axes bending is shown in Fig. 3.5. By dividing the magnitude of P by P_o and M by maximum moment (the value of moment generally near the balanced moment), a nondimensional graph of P/P_o vs. M/M_{max} can be drawn for each axis as shown in Figs. 3.6 and 3.7. Both graphs of Figs. 3.6 and 3.7 are similar to each other even for f'_c values that differ more than 800 psi. For both strong and weak axis interaction curves, only one graph can be used, and within the precision of rectangular stress block theory points on a skew bending interaction surface of rotation also would fit the one graph. From appropriate values of M/M_{max} for each of the thrust levels and for each principal axis either of the graphs of Figs. 3.6 or 3.7 can be used to develop the graph of Fig. 3.8 to represent the analytic estimate of capacity in terms of an interaction surface. For constant ratios P/P_o, the M/M_{max} graphs for the analytic capacity can be represented as a circular path in Fig. 3.8. The solid lines in Fig. 3.8 represent a contour of a circular interaction surface representing the analytic capacity for each of the thrust levels. Test results of all nine columns are also identified on the same graphs of Fig. 3.8. The points on the axis lines are the computed analytic capacity of the section shown in Fig. 3.8. The radius of each analytic circle represents the analytic uniaxial flexural capacity ratio for each thrust ratio.

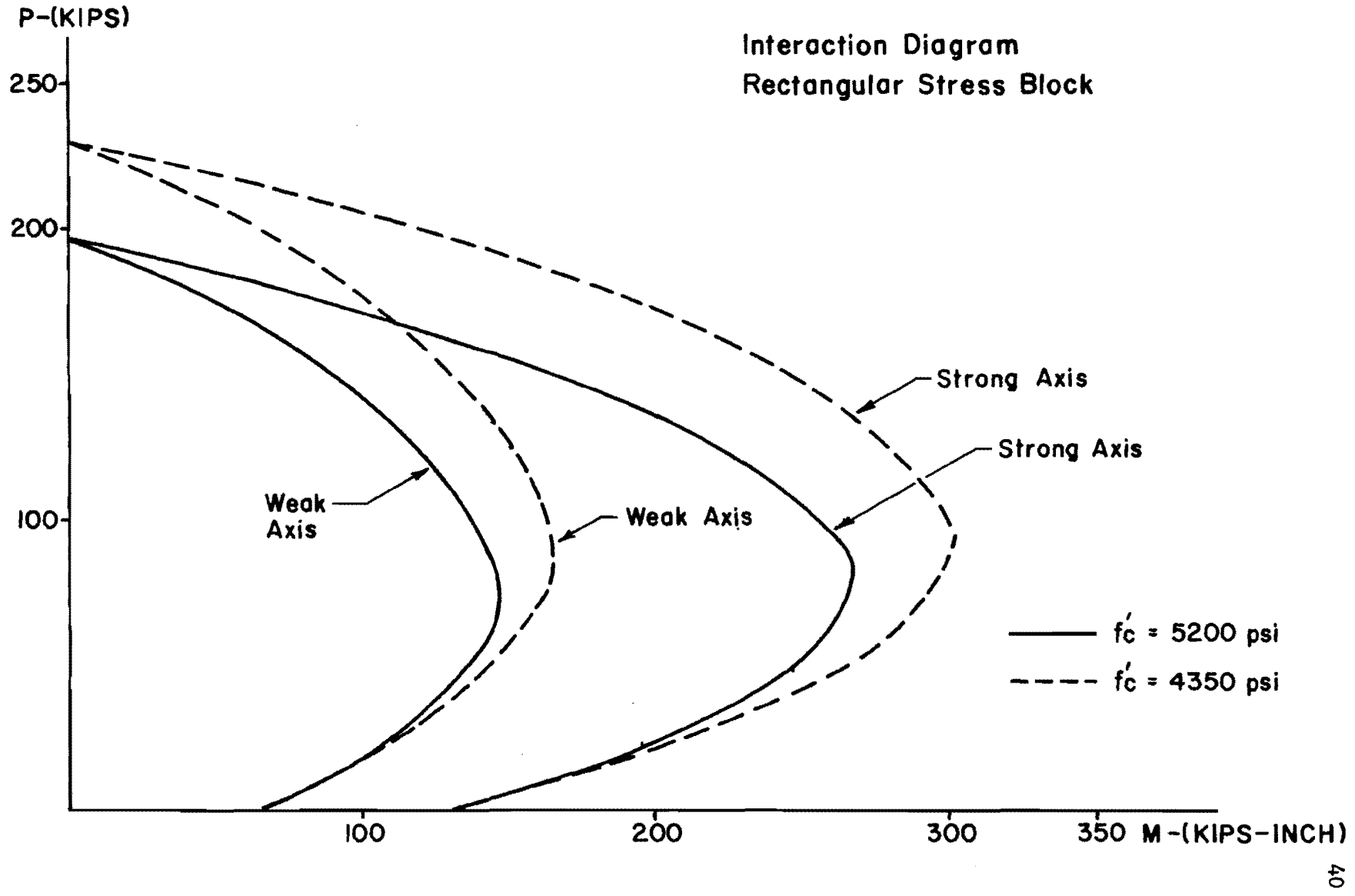

Fig. 3.5. Interaction diagram for maximum and minimum concrete strength.

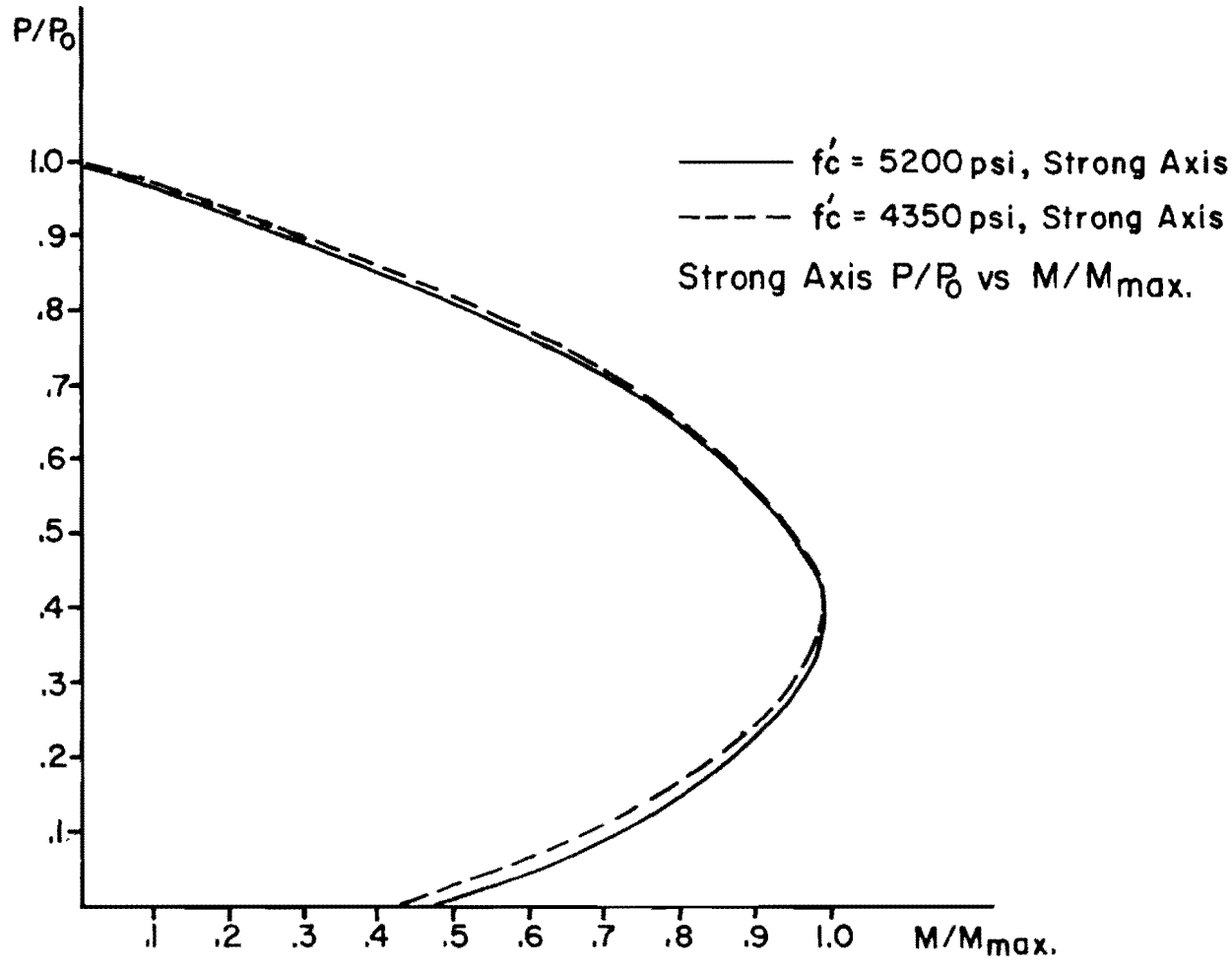

Fig. 3.6. Strong axis P/P_o vs. M/m_{max}.

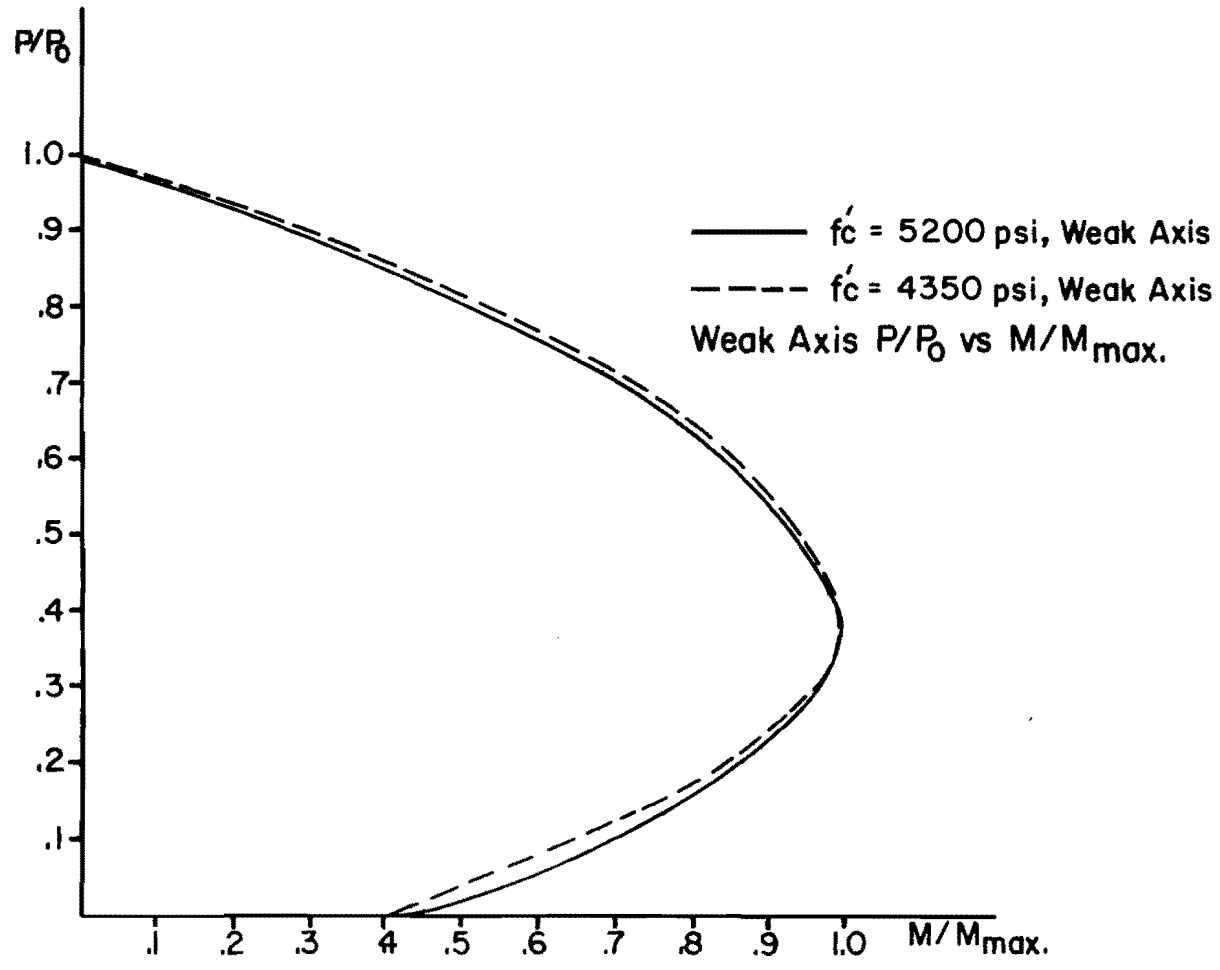

Fig. 3.7. Weak axis P/P_o vs. M/m_{max}.

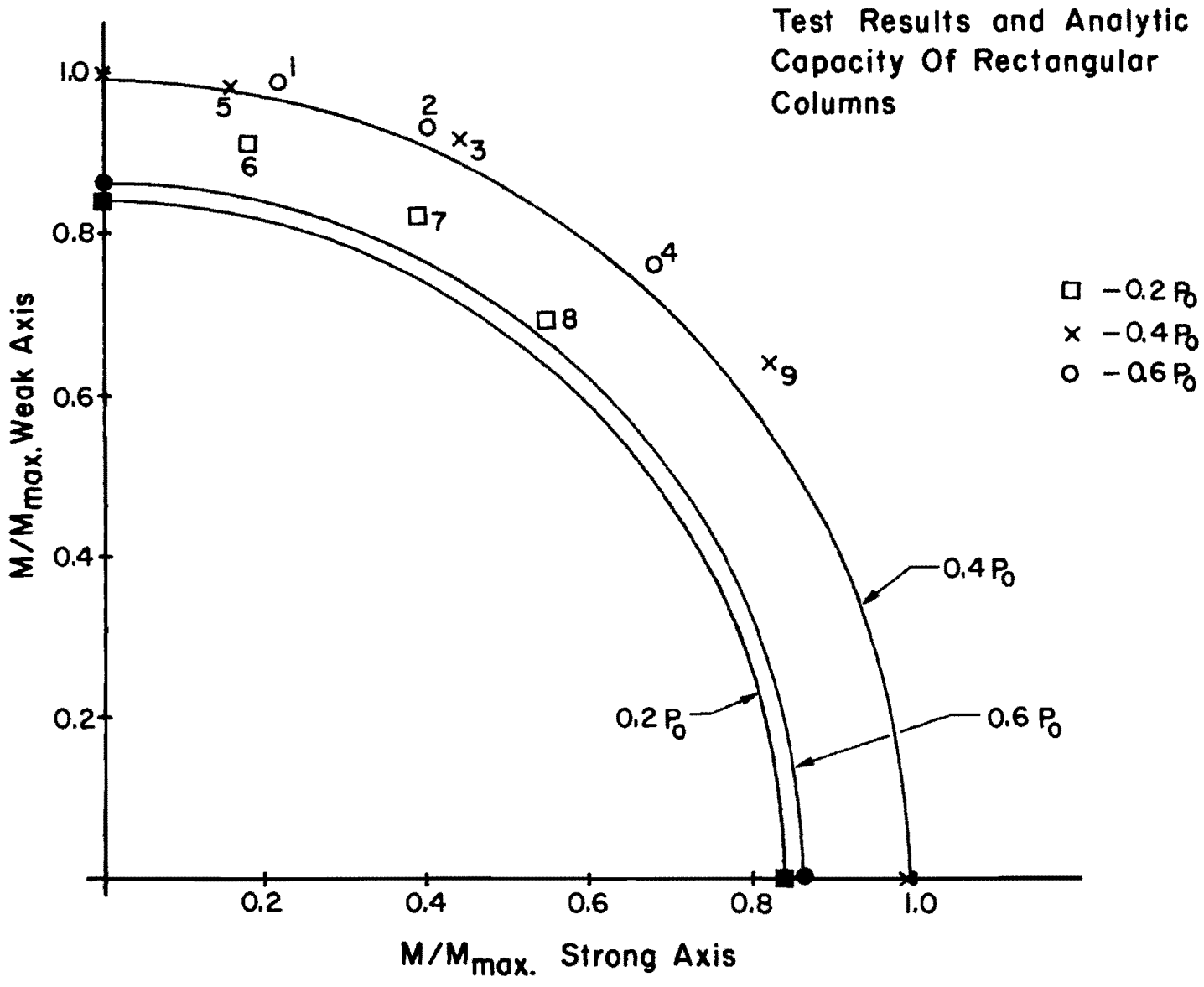

Fig. 3.8. Test results and analytic capacity of rectangular columns.

As seen from the graphs of Fig. 3.8, for thrusts of $0.2P_o$ (squares) and $0.4P_o$ (crosses) the surface of rotation fits measured data within 10 percent, while for thrusts of $0.6P_o$ (circles) measured strength exceeded the surface of rotation by about 17 percent. For the thrust level as high as $0.6P/P_o$, the use of a limit strain of 0.003 with the rectangular stress block to represent concrete strength could have underestimated uniaxial flexural capacity by as much as 10 percent if not more (Ref. [19], p. 29). The data indicate that the rectangular stress block representation of concrete strength tends to underestimate capacity as the thrust level reaches $0.6P/P_o$.

3.4 Maximum Compression Strain Before Failure

With each increment of load the strain and deflection in the column increased. The surface strain was measured by monitoring linear potentiometers as described in Section 2.4. The surface strain at each face was then translated into corner strains. The corner strain can be obtained from the equation of points in the plane defined by potentiometer displacements.

The specific detail for corner strain computation is explained by Green[16]. The southwest corner of column cross sections was the most highly compressed corner. The compressive strain which was measured at the midheight gage station is shown as a function of moment load in Fig. 3.9. Except for specimen RC-6 the maximum midheight corner compressive strain was computed to be greater than 0.0036 and lower than 0.0047 in./in. at ultimate load. The failure of specimen RC-6 occurred below midheight, before the measured midheight strain reached more than 0.0018. However, the ultimate strain at the station directly below midheight in Specimen RC-6 reached 0.005 in./in. as shown by the dashed line in Fig. 3.9. The maximum strain before failure exceeds the maximum values for each graph of Fig. 3.9 because the last data point for each graph represents the strain at maximum moment, not at the crushing, spalling stage of failure. All tests after RC-3 were terminated after the maximum moment had been reached (stage when flexural loading could not recover previous levels) in order to avoid

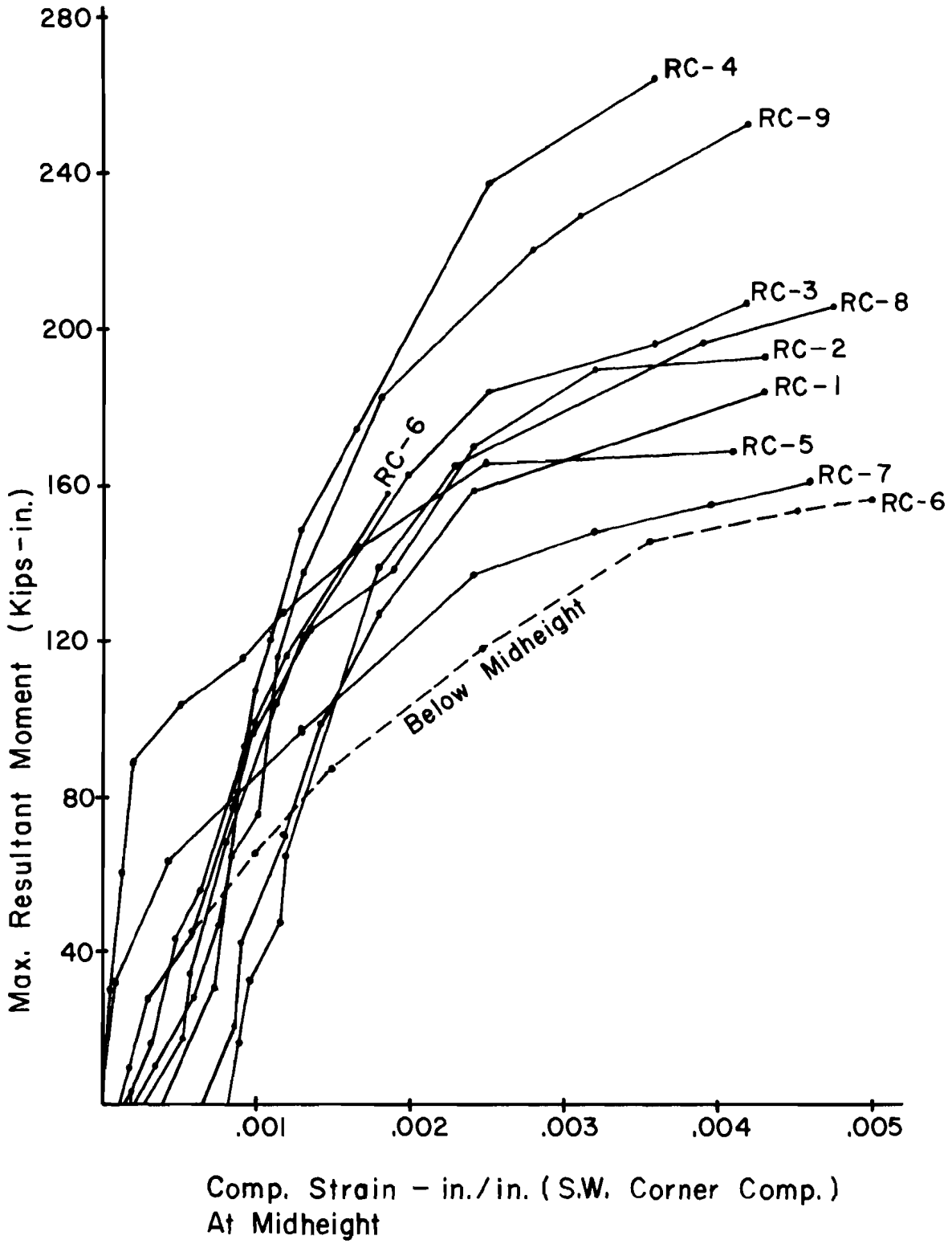

Fig. 3.9. Prefailure compressive strain at midheight vs. maximum resultant moment.

damaging the strain measuring equipment. The maximum centerline compressive and tensile strain measured at ultimate or failure load are recorded in Table 3.3.

3.5 Stiffness

During each test longitudinal displacement was measured opposite all four faces of the specimen and at five stations along the length of column. The measured displacement was transferred to the face of the column and then after conversion to strains, by using Eqs. (3.6) and (3.7) the curvature at each station was calculated as illustrated in Fig. 3.10.

$$\varphi_{ns} = \frac{\epsilon'_n - \epsilon'_s}{9.0} \tag{3.6}$$

$$\varphi_{ew} = \frac{\epsilon'_E - \epsilon'_w}{5.0} \tag{3.7}$$

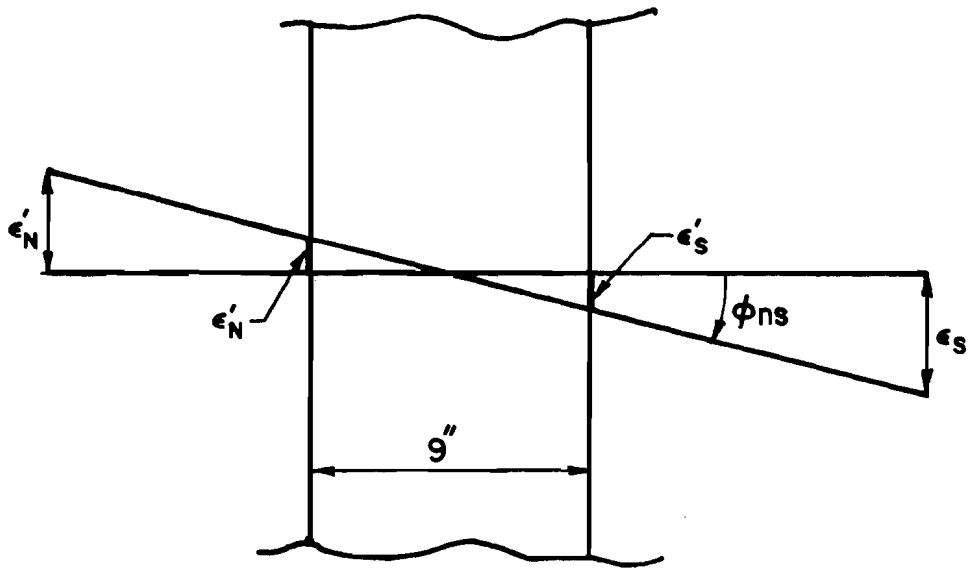

Fig. 3.10. Curvature representation.

A very small difference could be observed in the variation of moment among all five stations, but the amount of curvature differed greatly among all five stations. By taking an average curvature for all five stations, a graph of moment vs. average curvature was drawn. The graphs of moment vs. average curvature are shown in Figs. 3.11 through 3.19. The origin of graphs are taken from the load stage at which the first skew bending force was applied. The slope of the moment curvature graphs represent flexural stiffness.

Some nominal computed values of EI for uncracked sections about each axis are shown as lines of constant slope for each column. The value of E_c was taken as $57{,}400\sqrt{f'_c}$ psi and the gross moment of inertia for the cross section area was used.

Cracked section EI values were estimated as 40 percent of the gross EI values, and these lines also are shown as dashed lines. Each cracked section analytic stiffness line was drawn from an origin corresponding with the thrust at which the first crack was observed and recorded in the weak axis direction of bending. Using the moment at this load stage, the cracked section EI for weak axis stiffness was drawn in Figs. 3.11 through 3.19. It was not possible to differentiate between "first" cracks for strong axis bending and the simple extension of weak axis cracks, so no data were recorded for initial cracking due to strong axis bending. For the strong axis direction, a tensile strain recorded as greater than 0.0001 in./in. on the east face was used as an equivalent to initial cracking. In both the weak and the strong axes direction, cracked section EI was considered using ACI Eq. (10-7) and Eq. (10-8) [1,23].

$$EI = \frac{E_c I_g}{5} + E_s I_s \tag{3.8}$$

$$EI = \frac{E_c I_g}{2.5} \tag{3.9}$$

The effect of creep was ignored for analytic estimates of stiffness as the loading was essentially for short terms only during the tests. As others have reported, some creep or displacement under constant pressure was apparent at the highest levels of load.

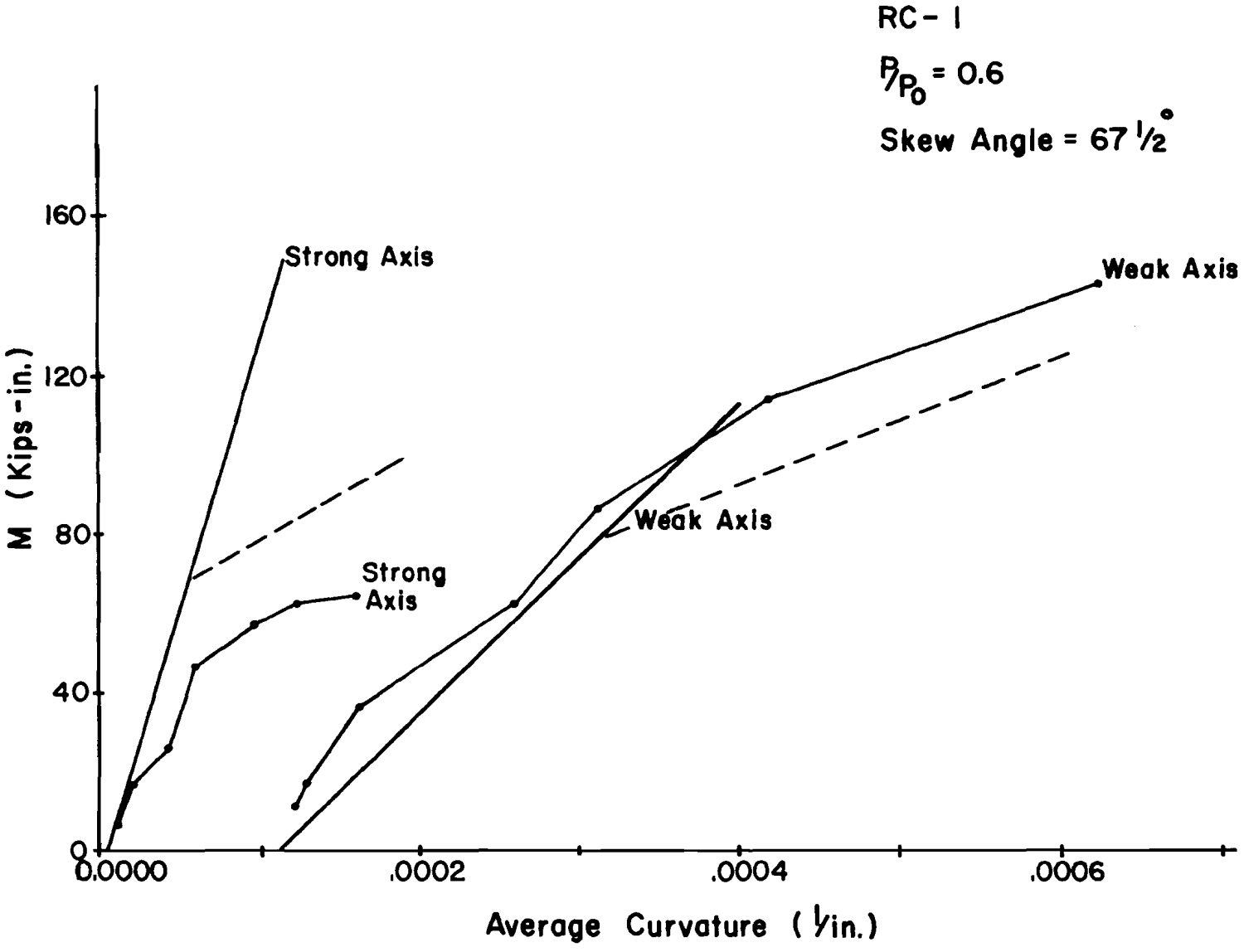

Fig. 3.11. Moment vs. average curvature RC-1.

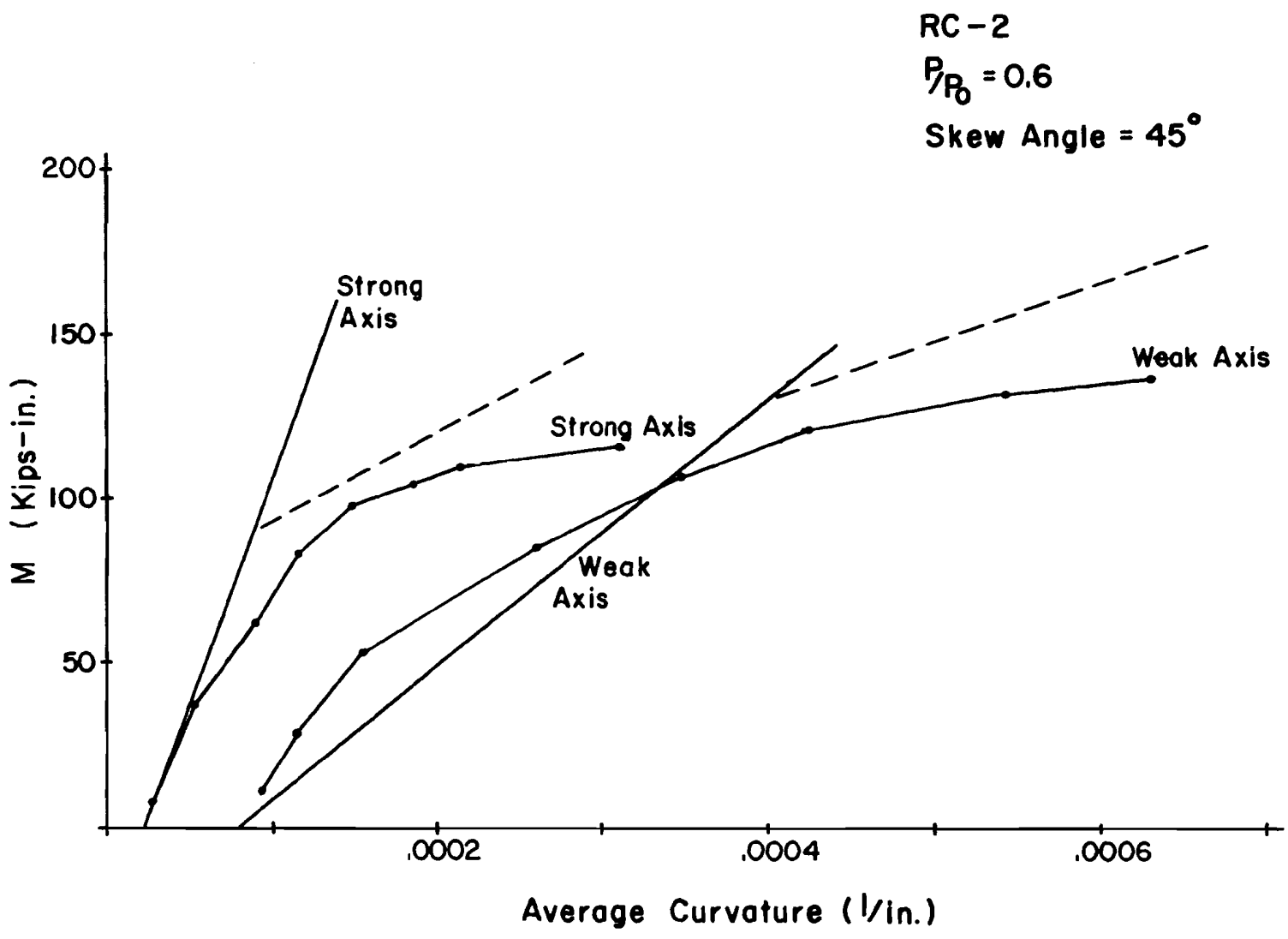

Fig. 3.12. Moment vs. average curvature RC-2.

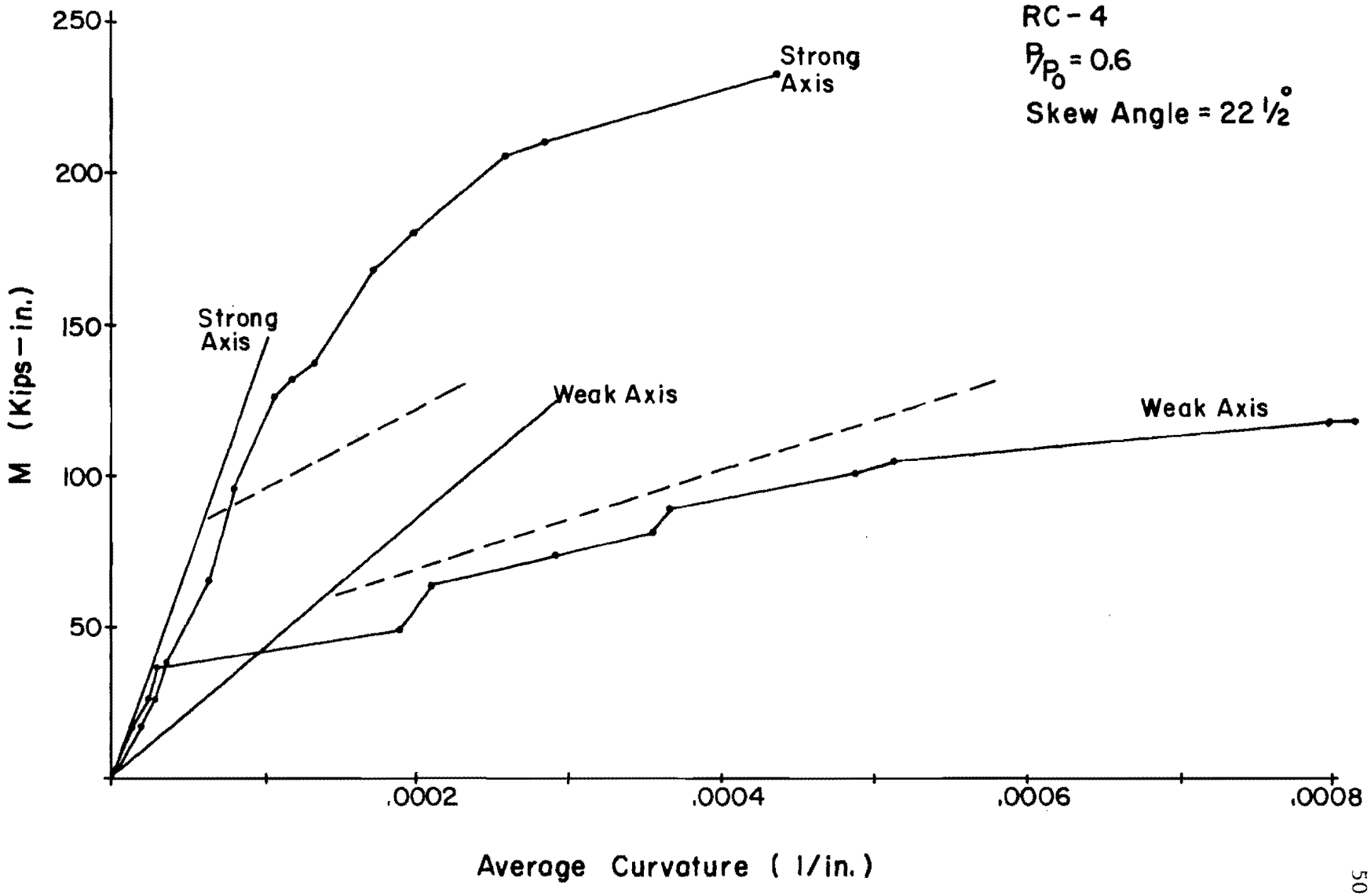

Fig. 3.13. Moment vs. average curvature RC-4.

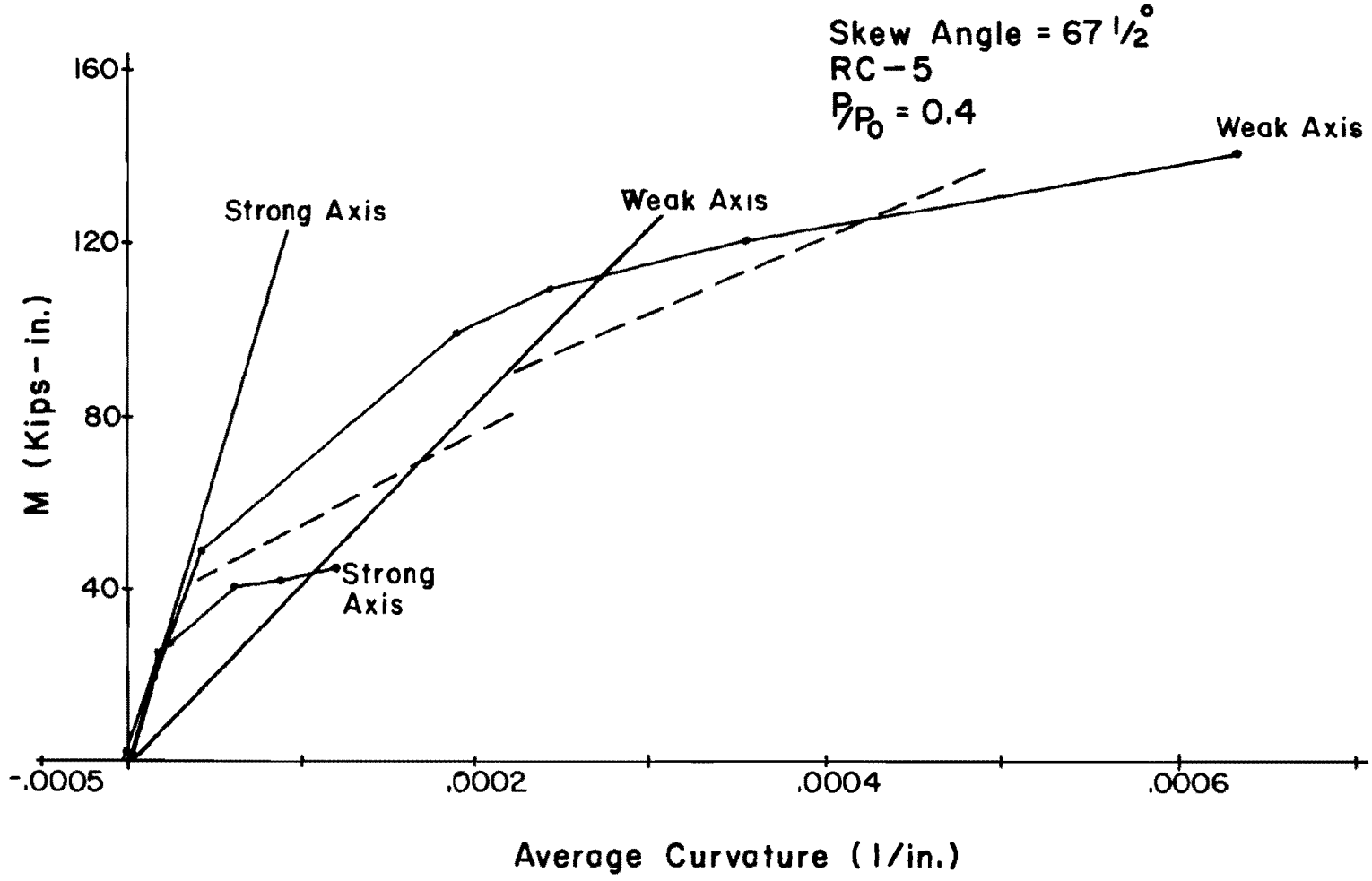

Fig. 3.14. Moment vs. average curvature RC-5.

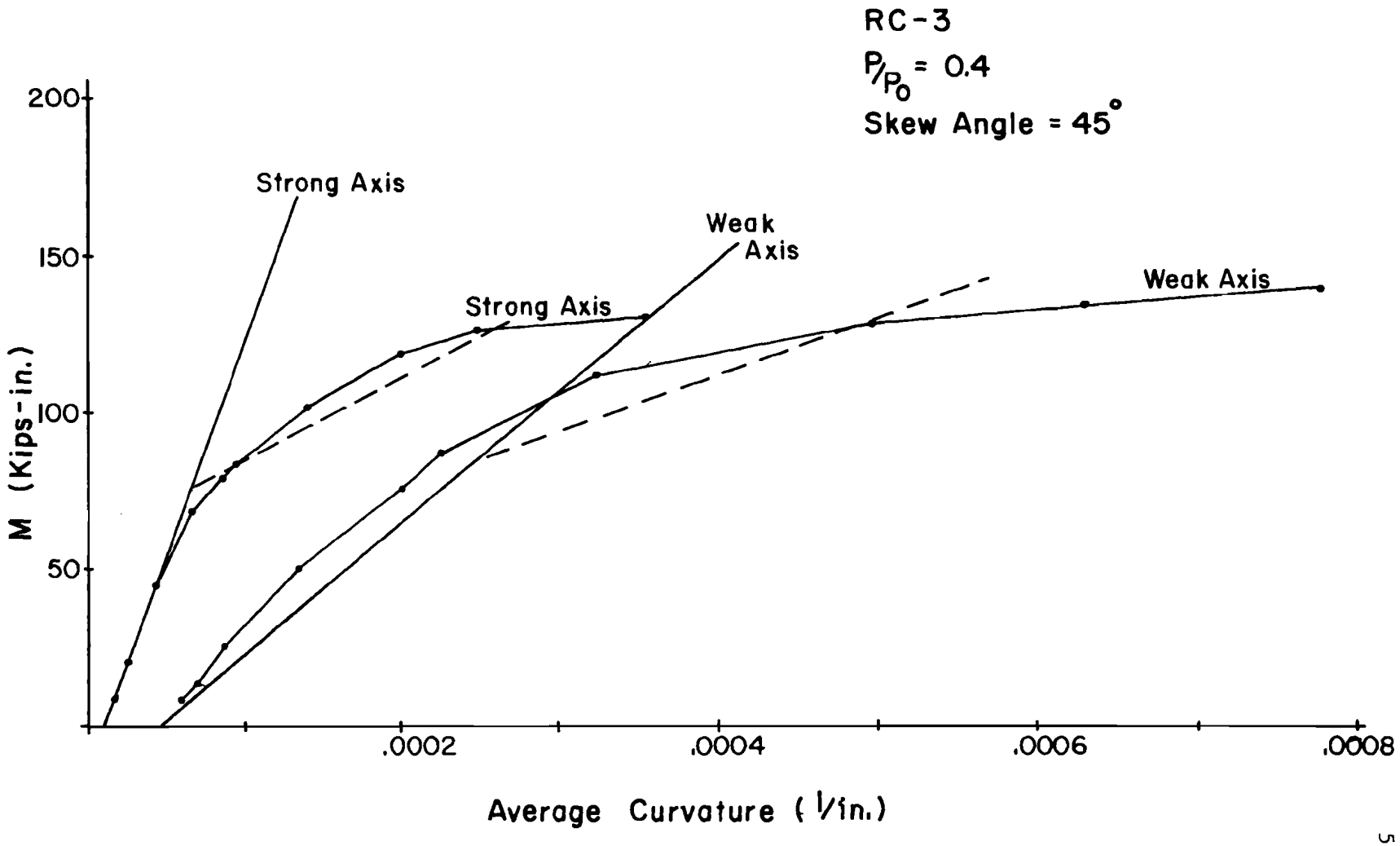

Fig. 3.15. Moment vs. average curvature RC-3.

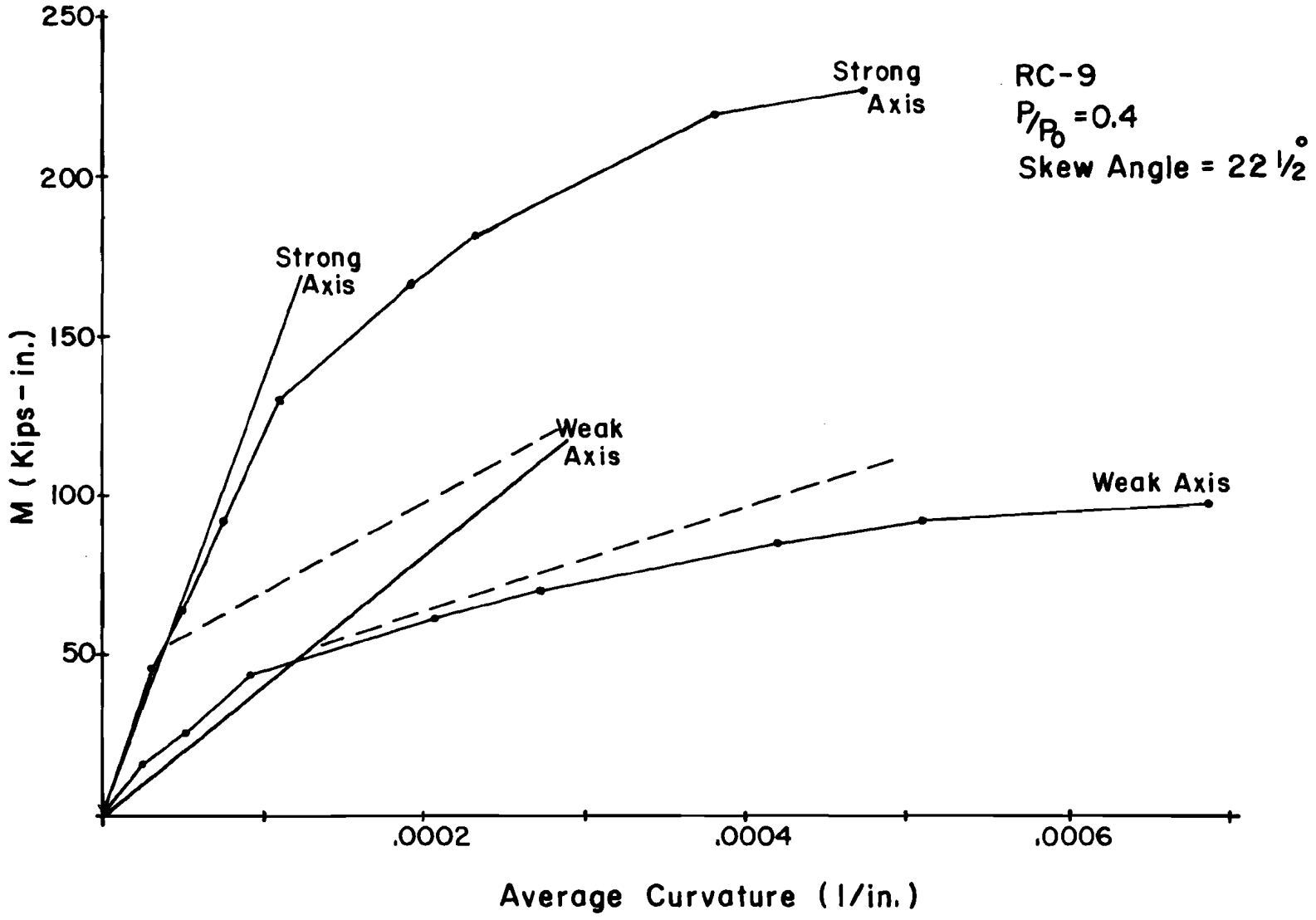

Fig. 3.16. Moment vs. average curvature RC-9.

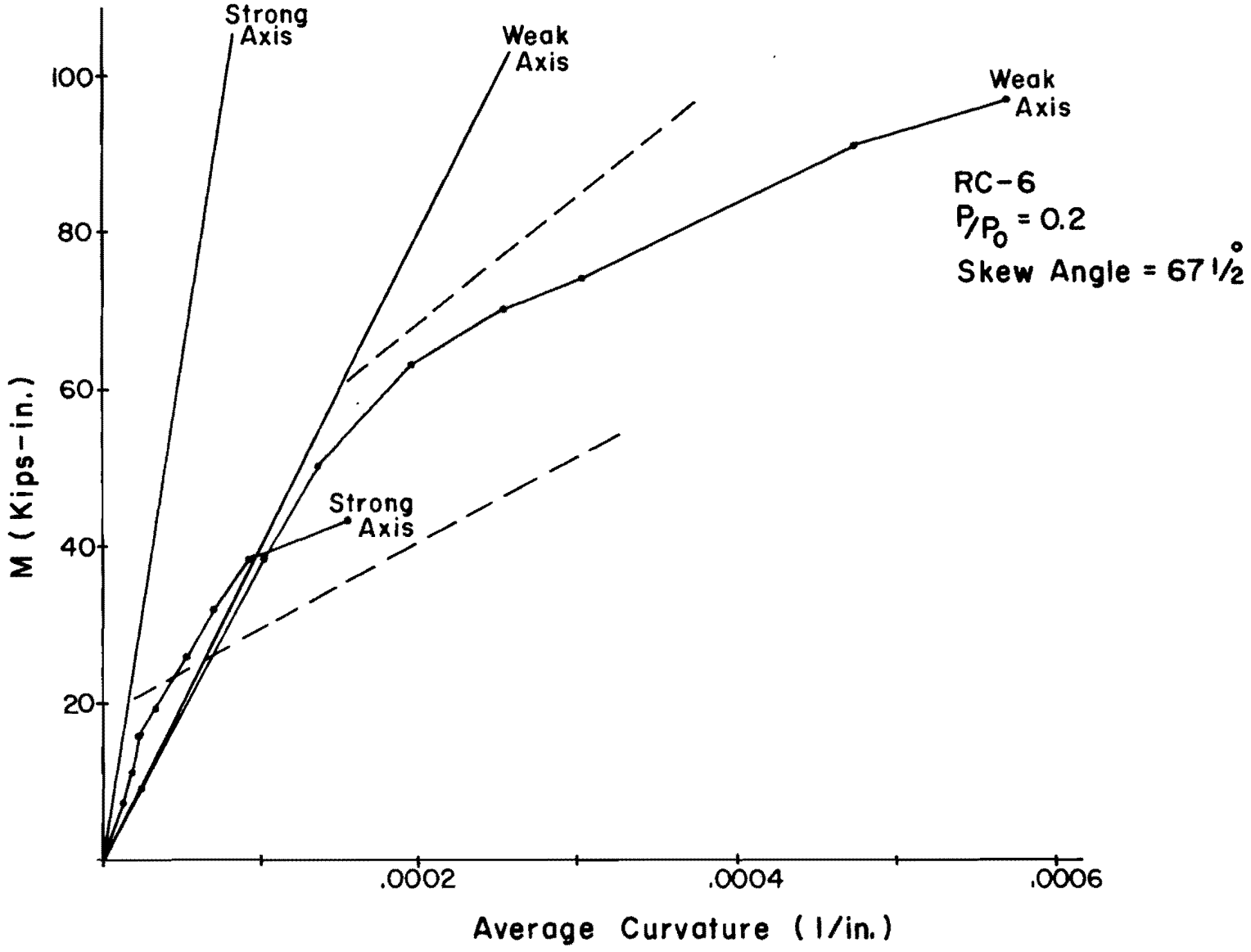

Fig. 3.17. Moment vs. average curvature RC-6.

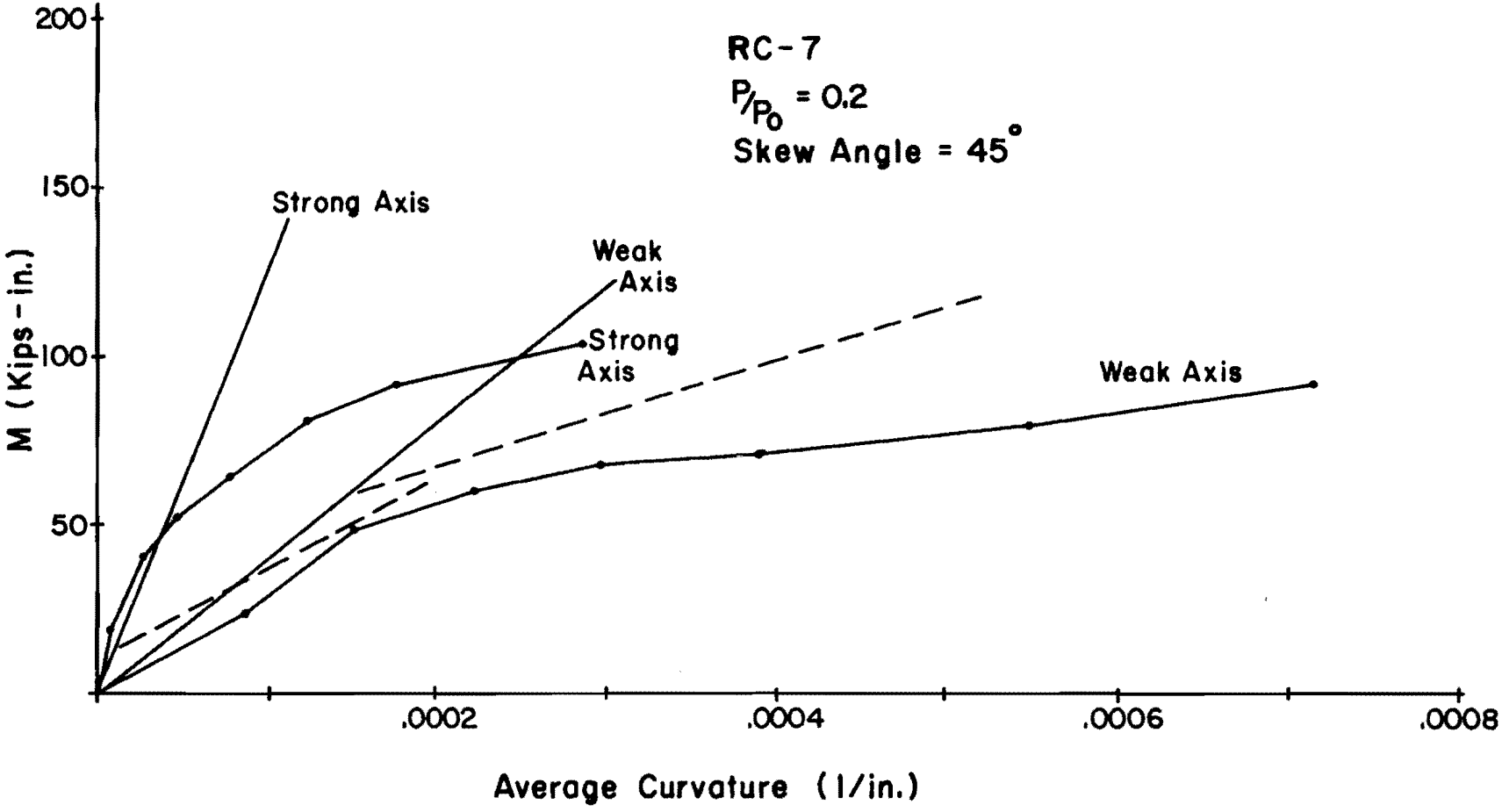

Fig. 3.18. Moment vs. average curvature RC-7.

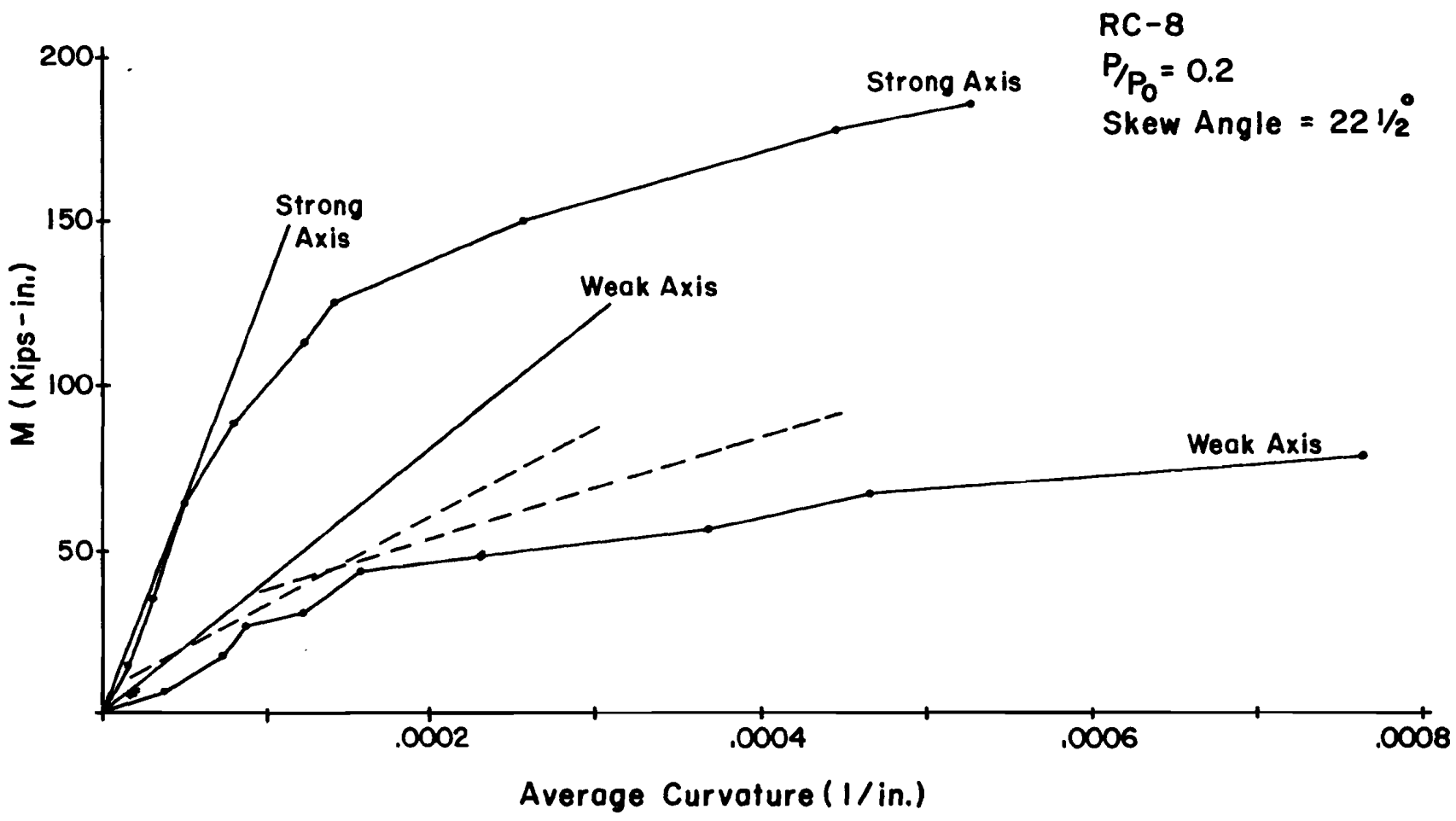

Fig. 3.19. Moment vs. average curvature RC-8.

The graphs indicate that for the columns subjected to low thrust of $0.2P_o$ (Figs. 3.17, 3.18, and 3.19), the nominal values of EI (the uncracked section EI) correspond well with the measured initial stiffness of columns. For the higher thrust ratios the correspondence between nominal EI and measured EI was even reasonably similar only for skew angles of 67.5^o and 45^o.

The measured stiffness decreased as moments reached levels adequate to crack the concrete. The graphs of Figs. 3.11 through 3.19 indicate that the values of cracked section EI for weak axis stiffness correspond vaguely with the measured stiffness for the low thrust level of $0.2P_o$ and for skew angle of 22.5^o at the higher thrust levels. However, the correspondence between computed and measured stiffness for the cracked section in the strong axis direction was not apparent. Flexural stiffness for strong axis bending appears to remain as stiff as for uncracked conditions until the tension surface strain is considerably in excess of 0.0001.

3.6 Moment Magnification Factors

Values of moment magnifier (δ_{ACI}) were calculated in accordance with the recommendations of the ACI Building Code [1],

$$\delta = \frac{C_m}{1 - \frac{P_u}{\varphi P_c}} \geq 1 \qquad (3.10)$$

where

$$P_c = \frac{\pi^2 EI}{(k\ell)^2} \qquad (3.11)$$

The values of C_m and φ were taken equal to unity in Eq. (3.10),' while values of $k\ell = 76$ were used for all specimens. The value of EI was taken as before from Eqs. (3.8) and (3.9) in calculations of P_c. In Eq. (3.10) the axial thrust level P_u was taken as P_{test} (Table 3.3). P_{test} was the maximum load that could be applied to the specimen to maintain the desired thrust level. The summary of calculations of δ_{ACI} for each specimen and for both the axes is tabulated in Table 3.4.

TABLE 3.4. MOMENT MAGNIFIER (δ)USING ACI EQ. (10-5)

Specimen	$E_c I_g$		$EI = E_c I_g/2.5$		$P_c = \pi^2 EI/(kL)^2$		$\delta = C_m/(1 - P/\phi P_c)$	
	Strong	Weak	Strong	Weak	Strong	Weak	Strong	Weak
RC-1	1223000	378000	490000	151000	836.03	256.24	1.166	1.859
RC-2	1221000	377000	488500	150800	828.98	255.88	1.168	1.876
RC-3	1263000	390000	505300	156000	857.44	264.64	1.128	1.555
RC-4	1260000	389000	504000	155500	854.96	263.91	1.176	1.942
RC-5	1239000	382400	495600	152900	840.94	259.55	1.115	1.500
RC-6	1164000	260000	465710	143700	790.23	243.90	1.072	1.279
RC-7	1154000	356000	461700	142500	783.42	241.79	1.052	1.190
RC-8	1167000	360200	467000	144075	792.08	244.47	1.053	1.196
RC-9	120000	370300	480000	148100	814.35	251.34	1.116	1.507

Specimen	$E_c I_g$		$EI = \frac{E_c I_g}{5} + E_s I_s$ *		$P_c = \pi^2 EI/(kL)^2$		$\delta = C_m/(1 - P/\phi P_c)$	
	Strong	Weak	Strong	Weak	Strong	Weak	Strong	Weak
RC-1	1223000	378000	378200	111500	646.24	190.5	1.23	2.67
RC-2	1221000	377000	377480	111400	645.96	190.35	1.22	2.72
RC-3	1263000	390000	385850	114000	659131	194.80	1.17	1.95
RC-4	1260000	389000	385200	113750	658.20	194.37	1.24	2.97
RC-5	1239000	382400	381000	112450	651.0	192.15	1.15	1.83
RC-6	1164000	260000	366055	107850	625.5	184.29	1.09	1.41
RC-7	1154000	356000	364050	107250	622.1	183.26	1.07	1.27
RC-8	1167000	360200	366700	10803	626.6	184.61	1.07	1.28
RC-9	120000	370300	373200	110050	637.7	188.05	1.15	1.83

*$E_s I_s$ - Strong Axis = 133200 ksi, Weak Axis = 36000 ksi.

A comparison of these calculated values of δ_{ACI} with the values of measured values $\delta_{measured}$ was desired. The magnitude $\delta_{measured}$ was calculated by taking the ratio of the total midheight moment to the end moment for maximum load conditions on each specimen.

The values of $\delta_{measured}$ vs. δ_{ACI} are tabulated in Table 3.5 for each specimen and for bending about each major axis. The comparison indicates that at the thrust level of $0.6P_o$, the ACI procedure gives higher values of δ than the measured values, while at the lower thrust level of $0.2P_o$ the measured values of δ are higher. Possibly the lower values for δ_{ACI} at lower thrust levels should have included an allowance for creeping of concrete. The introduction of a quantity for the factor βd may improve the correlation of results, but the evaluation of creep effects was considered to be beyond the scope of this study. The significance of ratios $\delta_{measured}$ vs. δ_{ACI} less than unity could be interpreted to mean that the suggested procedure for magnification factors is unconservative when axial loads are as low as $0.2P_o$.

Listed in Table 3.6 are the resultants of measured moments for comparison with the resultants of magnified moments in accordance with Eq. (3.12) and recommendations of Section 10.11.5.2 of the ACI Building Code.

$$\sqrt{(\delta_{wACI} M_{uw})^2 + (\delta_{sACI} M_{us})^2} = M_{RACI} \qquad (3.12)$$

where

δ_{wACI} = moment magnifier for weak axis (Table 3.4).

δ_{sACI} = moment magnifier for strong axis (Table 3.4).

M_{uw} and M_{us} = primary moment for weak and strong axis (Table 3.5).

M_{RACI} = resultant magnified moment

M_R = resultant measured moment

Again, the ratios between measured and computed skew bending moments indicate that at the high thrust level of $0.6P_o$, ACI Eq. (10-8) gives higher values. At the lower thrust level of $0.2P_o$, ACI Eq. (10-8) did not appear

TABLE 3.5. COMPARISON OF $\delta_{measured}$ VS. δ_{ACI}

Thrust Level P/P_o	RC	P_{test} kips	$\frac{P_{test}}{P_o}$	Measured Moments				Weak Axis			Strong Axis		
				Primary		Secondary		$\delta_{meas.}$	δ_{ACI}		$\delta_{meas.}$	δ_{ACI}	
				Weak	Strong	Weak	Strong						
0.6	1	119.2	0.544	123.7	57.4	193.5	72.3	1.564	1.859	(2.67)*	1.260	1.166	(1.23)
	2	120.3	0.551	90.4	107.4	157.8	124.4	1.746	1.876	(2.72)	1.158	1.168	(1.22)
	4	128.9	0.556	70.0	194.5	136.4	229.7	1.949	1.942	(2.97)	1.181	1.176	(1.24)
0.4	3	95.1	0.411	89.7	113.1	164.9	133.0	1.838	1.555	(1.95)	1.176	1.128	(1.17)
	5	87.1	0.389	91.1	49.8	154.9	53.1	1.700	1.50	(1.83)	1.066	1.115	(1.15)
	9	85.05	0.401	64.2	186.9	98.0	210.6	1.526	1.507	(1.83)	1.129	1.116	(1.15)
0.2	6	53.5	0.266	94.0	47.5	136.9	53.7	1.456	1.279	(1.41)	1.131	1.072	(1.09)
	7	38.9	0.196	87.4	96.2	119.2	105.4	1.363	1.190	(1.27)	1.096	1.052	(1.07)
	8	40.4	0.200	65.9	175.6	87.8	191.2	1.332	1.196	(1.28)	1.196	1.053	(1.07)

*Values in parentheses are those determined for ACI Eq. (10-7) and the others are determined with ACI Eq. (10-8).

TABLE 3.6. M_R VS. M_{RACI}

(a) Using Eq. (10-7)

Through Level P/P_o	Specimen	M_R k-in.	M_{RACI} k-in.	$\frac{M_{RACI}}{M_R}$
0.6	RC-1	197.4	337.7	1.71
	RC-2	198.5	278.62	1.40
	RC-4	263.5	318.42	1.21
0.4	RC-3	207.9	189.0	0.91
	RC-5	160.4	176.28	1.10
	RC-9	230.4	244.95	1.06
0.2	RC-6	145.4	142.29	0.98
	RC-7	156.7	151.38	0.97
	RC-8	209.1	205.96	0.99

(b) Using Eq. (10-8)

Through Level P/P_o	Specimen	M_R k-in.	M_{RACI} k-in.	$\frac{M_{RACI}}{M_R}$
0.6	RC-1	197.4	239.5	1.21
	RC-2	198.5	210.9	1.06
	RC-4	263.5	266.1	1.01
0.4	RC-3	207.9	189.0	0.91
	RC-5	160.4	147.5	0.92
	RC-9	230.4	229.9	1.00
0.2	RC-6	145.4	130.6	0.90
	RC-7	156.7	145.1	0.93
	RC-9	209.1	201.0	0.96

to provide for enough magnification of moment. ACI Eq. (10-7) appeared to provide too much moment magnification at high thrust levels, but at the lower thrust level it provided for magnification factors almost the same as those measured. With extensive tensile cracking before failure at the lower thrust level, it does seem reasonable that the equation that contains recognition of reinforcement for stiffness should provide more reliable evidence of slenderness effects. Even with the relatively low reinforcement ratio of 0.011, Eq. (10-7) should be recommended when the thrust level is less than P_{bal}.

C H A P T E R I V

CONCLUSIONS

The objective of this report was to review and interpret the results of tests performed on rectangular columns subjected to axial compressive force and biaxial bending. Results regarding strength, maximum compressive strain in concrete and stiffness are reported.

The tests reported in this thesis included only rectangular cross sections with a reinforcement ratio ρ_g = 1.1 percent. Concrete strength varied from 4300 psi to 5200 psi. Axial thrusts of $0.2P_o$, $0.4P_o$ and $0.6P_o$ were maintained as biaxial flexural forces were applied. The nominal skew loading angles for flexural forces were 22.5^o, 45^o and 67.5^o. From the results of these tests and interpretation of results, the following observations are made:

1. The flexural strength of the rectangular columns subjected to biaxially eccentric thrust can be described by an elliptical function relating the ratios between skew moment components and uniaxial moment capacities. The function is shown as Eq. (4.1), and it can be used for checking the strength of cross sections.

$$\left(\frac{M_x}{M_{xmax}}\right)^2 + \left(\frac{M_y}{M_{ymax}}\right)^2 = 1.0 \qquad (4.1)$$

where

M_x, M_y = moment components in major and minor axes

M_{xmax}, M_{ymax} = uniaxial moment capacities in major and minor axes

2. The maximum strain of 0.0038 in./in. in concrete suggested by Hognestad seems reasonable as in all nine column tests the ultimate failure strain was not less than 0.0033 in./in. nor greater than 0.0048 in./in.

3. The flexural stiffness of cross sections can be represented by the analytic value of the product E_c and I_g only for loads that are less than 25 percent of section capacity while the section remains uncracked.

4. At high thrust levels the ACI method of magnifying individual moments for both principle axes in order to obtain a resultant moment for design is safe. But at low thrust levels the ACI method tends to underestimate the total amount of magnified moment near the point of maximum lateral deflection. ACI Eq. (10-7) provides much better estimates of the slenderness effect than does ACI Eq. (10-8) at low thrust levels.

R E F E R E N C E S

1. American Concrete Institute, Committee 318 ACI Standard Building Code Requirements for Reinforced Concrete (ACI 318-71), American Concrete Institute, Detroit, Michigan, 1971.

2. Craemer, Hermann, "Skew Bending in Reinforced Concrete Computed by Plasticity," ACI Journal, Vol. 23, No. 6, Feb. 1952, pp. 516-519.

3. Au, Tung, "Ultimate Strength Design of Rectangular Concrete Members Subject to Unsymmetrical Bending," ACI Journal, Vol. 29, No. 8, February 1958, pp. 657-674.

4. ACI-ASCE Joint Committee on Ultimate Strength Design, "Report on Ultimate Strength Design," ASCE Proc.-Separate 908, October 1955.

5. Chu, K. M., and Pabarccius, A., "Biaxially Loaded Reinforced Columns," Proceeding, ASCE Journal of Structural Division, Vol. 85, St. 5 June 1959, pp. 47-54.

6. Bresler, Boris, "Design Criteria for Reinforced Columns under Axial Load and Biaxial Bending," ACI Journal, Vol. 32, No. 5, November 1960, pp. 481-490.

7. Furlong, R. W., "Ultimate Strength of Square Columns under Biaxially Eccentric Loads," ACI Journal, Vol. 32, No. 9, March 1961, pp. 1129 - 1140.

8. Pannell, F. N., "Failure Surfaces for Members in Compression and Biaxial Bending," ACI Journal, No. 1, January 1963, pp. 129 - 140.

9. Pannell, F. N. Discussion, ASCE Journal of Structural Division, Vol. 85, St. 6, June 1959, pp. 47-51.

10. Ramamurthy, L. N., "Investigation of the Ultimate Strength of Square and Rectangular Columns under Biaxially Eccentric Loads," American Concrete Institute Special Publication SP-13, Paper No. 13, 1966.

11. Brettle, N. J., and Warner, R. F., "Ultimate Strength Design of Rectangular Reinforced Concrete Sections in Compression and Biaxial Loading," Civ. Eng. Tras. I. I. Austria, Vol. CE 10, No. 6, April 1968, pp. 101-110, (Paper No. 2470).

12. Warner, R. F., "Biaxial Moment Thrust Curvature Relations," ASCE Journal of Structural Engineering, ST5, May 1959, pp. 923 or New South Wales University, Sydney, Australia Report No. R-28, January 1968.

13. Redwine, R. B., "The Strength and Deformation Analysis of Rectangular Reinforced Concrete Columns in Biaxial Bending, unpublished M.S. thesis The University of Texas at Austin, May 1974.

14. Farah, Anis and Huggins, M. W., "Analysis of Reinforced Concrete Columns Subjected to Longitudinal Load and Biaxial Bending," ACI Journal, July 1969, pp. 569-575.

15. Fleming R. J., "Ultimate Strength Analysis for Skew Bending of Reinforced Concrete Columns," unpublished M.S. thesis, The University of Texas at Austin, May 1974.

16. Green, D. J., "Physical Testing of Reinforced Concrete Columns in Biaxial Bending," unpublished M.S. thesis, The University of Texas at Austin, May 1975.

17. Chang, W. F., "Long Restrained Reinforced Concrete Columns," unpublished Ph.D. dissertation, The University of Texas at Austin, June 1961.

18. Breen, J. E., "The Restrained Long Concrete Column as a Part of a Rectangular Frame," unpublished Ph.D. dissertation, The University of Texas at Austin, June 1962.

19. Furlong, R. W., "Long Columns in Single Curvature as a Part of Concrete Frames, unpublished Ph.D. dissertation, The University of Texas at Austin, June 1963.

20. Green, Roger, "Behavior of Unrestrained Reinforced Concrete Columns under Sustained Load," Ph.D. dissertation, The University of Texas at Austin, January 1966.

21. Texas Highway Department, "Standard Specifications for Road and Bridge Construction," January 1962.

22. Timoshenko, S. P., and Gere, J. M., Theory of Elastic Stability, McGraw-Hill Book Co., Second Edition, 1961.

23. American Concrete Institute, Committee 318, Commentary on Building Code Requirements for Reinforced Concrete (ACI 318-71), Detroit, Michigan, ACI, 1971.

24. PCA-Advanced Engineering Bulletin 18, "Capacity of Reinforced Concrete Rectangular Columns Subjected to Biaxial Bending," Chicago, Illinois, 1966.

25. PCA-Advanced Engineering Bulletin 20, "Biaxial and Uniaxial Capacity of Rectangular Columns," Chicago, Illinois, 1966.

26. Hognestad, E., "A Study of Combined Bending and Axial Load in Reinforced Concrete Members," Bulletin No. 399, University of Illinois Engineering Experiment Station, Urbana, November 1951, p. 28.

27. Whitney, C. S., "Design of Reinforced Concrete Members under Flexure or Combined Flexure and Direct Compression, ACI Journal, March-April 1937, pp. 483-498.

28. CRSI Handbook Based upon the 1971 ACI Building Code, Concrete Reinforcing Steel Institute, 1972.

29. Fowler, Timothy, J., "Reinforced Concrete Columns Governed by Concrete Compression," CESRL Dissertation No. 66-2, January 1966, Department of Civil Engineering, The University of Texas at Austin.